SANDIA REPORT

SAND2005-5023
Unlimited Release
Printed September, 2005

High-Speed Micro-Electro-Discharge Machining

Shawn P. Moylan, Srinivasan Chandrasekar, Gilbert L. Benavides

Prepared by
Sandia National Laboratories
Albuquerque, New Mexico 87185 and Livermore, California 94550

Sandia is a multiprogram laboratory operated by Sandia Corporation,
a Lockheed Martin Company, for the United States Department of Energy's
National Nuclear Security Administration under Contract DE-AC04-94AL85000.

Issued by Sandia National Laboratories, operated for the United States Department of Energy by Sandia Corporation.

Available to DOE and DOE contractors from
U.S. Department of Energy
Office of Scientific and Technical Information
P.O. Box 62
Oak Ridge, TN 37831

Telephone: (865)576-8401
Facsimile: (865)576-5728
E-Mail: reports@adonis.osti.gov
Online ordering: http://www.osti.gov/bridge

Available to the public from
U.S. Department of Commerce
National Technical Information Service
5285 Port Royal Rd
Springfield, VA 22161

Telephone: (800)553-6847
Facsimile: (703)605-6900
E-Mail: orders@ntis.fedworld.gov
Online order: http://www.ntis.gov/help/ordermethods.asp?loc=7-4-0#online

SAND2005-5023
Unlimited Release
Printed September 2005

High-Speed Micro-Electro-Discharge Machining

Shawn P. Moylan
Dr. S. Chandrasekar

School of Industrial Engineering
Purdue University
West Lafayette, IN 47906

and

Gilbert L. Benavides

Sandia National Laboratories
P.O. Box 5800
Albuquerque, NM 87185

Abstract

When two electrodes are in close proximity in a dielectric liquid, application of a voltage pulse can produce a spark discharge between them, resulting in a small amount of material removal from both electrodes. Pulsed application of the voltage at discharge energies in the range of micro-Joules results in the continuous material removal process known as micro-electro-discharge machining (micro-EDM). Spark erosion by micro-EDM provides significant opportunities for producing small features and micro-components such as nozzle holes, slots, shafts and gears in virtually any conductive material. If the speed and precision of micro-EDM processes can be significantly enhanced, then they have the potential to be used for a wide variety of micro-machining applications including fabrication of microelectromechanical system (MEMS) components. Toward this end, a better understanding of the impacts the various machining parameters have on material removal has been established through a single discharge study of micro-EDM and a parametric study of small hole making by micro-EDM. The main avenues for improving the speed and efficiency of the micro-EDM process are in the areas of more controlled pulse generation in the power supply and more controlled positioning of the tool electrode during the machining process. Further investigation of the micro-EDM process in three dimensions leads to important design rules, specifically the smallest feature size attainable by the process.

Contents

Figures

Tables

1. Introduction

When two electrodes are in close proximity in a dielectric liquid, application of a voltage pulse between them can break down the dielectric and produce a spark discharge between the electrodes. Some of the energy in the discharge is transferred to the electrodes and results in the heating of highly localized regions of the electrodes. If the regions are heated above their melting or vaporization temperature, molten droplets or vaporized material may be ejected from the electrodes. Repetitive pulsing of the voltage results in repeated breakdown of the dielectric and material removal, and consequently to a continuous machining process called Electrical Discharge Machining (EDM). Since the melting/vaporization temperature, and not hardness, of the electrode materials controls material removal, EDM has proved enormously beneficial for machining complex shapes in hard materials that are difficult to fabricate by conventional means. A variant of the EDM process is micro-EDM, so called because it utilizes low discharge energies ($\sim 10^{-9} - 10^{-5}$ Joules) to remove small volumes ($\sim 0.05 - 500\ \mu m^3$) of material. This small volumetric removal means micro-EDM provides significant opportunities for producing small features and micro-components such as nozzle holes, slots, shafts and gears in any conductive material – hard alloys, advanced ceramics, very rapidly solidified micro-powders, and colloidal suspensions among other materials. If the speed and precision of micro-EDM processes can be significantly enhanced, then they have the potential to be used for a wide variety of micro-machining applications with functional materials including fabrication of micro-electro-mechanical system (MEMS) components. It is these topics that constitute the core of the proposed research.

This study seeks to demonstrate improved machining times with the micro-EDM process and to quantify the smallest feature that can be machined using state-of-the-art micro-EDM technology. While there are several routes to improving machining time, many sacrifice precision or accuracy to do so. High-speed micro-EDM will only be achieved by improving machining times with minimal trade-off. An important aspect of this study will be to understand and to characterize this trade-off, and to investigate methods of reducing machining times while maintaining high levels of precision. Additionally, prior literature has illustrated some very

small features created by the micro-EDM process; yet none has discussed why smaller features cannot be achieved. An estimate of the smallest feature size realizable by EDM has not been made. Preliminary experiments conducted for the present study indicate that discharge energy and size of the tool electrode are dominant parameters limiting the smallest feature. An attempt will be made to estimate the minimum feature size attainable and its dependence on discharge energy and electrode size.

The goals stated above will be accomplished by first characterizing the state-of-the-art in micro-EDM through a thorough literature survey of the subject and testing of existing micro-EDM systems. Following this, simple correlations between material removal and machining parameters will be obtained through two different methods: examining craters produced by a single discharge of micro-EDM, and a preliminary parametric study using machining time along with hole size and shape as metrics. These experiments will reveal the machining parameters that most influence important machining outputs, especially material removal rates. Potential areas of significant improvement to micro-EDM cycle times appear to be in power supply and in tool positioning. A novel experimental setup using a transistor based pulse power supply and a dual-level servo positioning system will seek to exploit this potential. Process performance while vibrating the tool electrode in open loop will be compared, in terms of material removal rate, feature size and shape, with performance when positioning the tool with closed-loop feedback of discharge conditions. Not only will one-dimensional machining of holes be investigated, but two-dimensional machining of parallel slots will be used to demonstrate minimum feature sizes. Varying tool size and discharge energy when cutting parallel slots will provide a map of minimum features attainable as a function of micro-EDM parameters. This data, combined with the results of single discharges at very small energies, will enable an estimation of minimum feature sizes as a function of discharge energy and tool electrode dimensions.

2. Background

2.1 Literature Review

To gain a full appreciation of the state of the art in micro-EDM, 50+ research papers on the subject were read and analyzed. It is believed that these papers comprise the most significant of English language papers on the subject of micro-EDM. To appropriately summarize the papers and apply them to the research intended for this study, the same six questions were asked of each paper. What is the definition of micro-EDM? What are the strengths and weaknesses of the micro-EDM process? What types of parts are being machined by micro-EDM and in what materials are they being machined? What is the minimum feature size being machined? How quickly are the parts being made or what is the machining rate? What is the unique aspect of the research that improves the micro-EDM process? Every paper does not have an answer to every question, and often times the answers are a bit contradictory.

However, almost all of the papers agree on the second question. The main strength of the micro-EDM process is that it can machine complex shapes into ANY conductive material with very low forces. The forces are very small because the tool and the workpiece do not come into contact during the machining process. There are two very important weaknesses to the micro-EDM process. The first is that it is a rather slow machining process. Not only are material removal rates rather low compared to other machining and micro-machining processes, but micro-EDM is also a serial process, while other micro-machining processes, e.g. semi-conductor silicon processes, are parallel processes producing multiple, often times hundreds, of parts in one cycle. The second weakness is that while the workpiece electrode is being machined, the tool electrode also wears at a rather significant rate. This tool-wear leads to shape inaccuracies.

The result of all papers having similar answers to the strength/weakness question is that most of the research focuses on one of only a few subjects. The research papers can be filed into one of three categories: attempting to improve the speed of micro-EDM, attempting to improve the accuracy or shape-complexity of micro-EDMed parts, and attempting to apply the micro-EDM process to new types of component fabrication. Interestingly, the research in each paper is

largely confined to only one of the three subjects, almost totally disregarding the other two subjects. The following sub-sections discuss research done in each of the three mentioned areas.

2.1.1 Improving the speed of the micro-EDM process

All of the encountered research focusing on improving the speed of micro-EDM fixated on the fact that part throughput is limited by the fact that micro-EDM is a serial process. Silicon fabrication processes, mainly lithography and etching, dominate the micromachining field. By using various masks and etchants, a large number of complex shapes can be processed into one silicon wafer. In fact, one wafer can often yield hundreds, even thousands, of parts or individual micro-machines. With this as the operating norm, it is difficult for a serial process like micro-EDM to gain respect in the micromachining field.

One of the first efforts to make the micro-EDM process more parallel recognized that the majority of jobs performed by micro-EDM (at the time) were drilling multiple holes into a part. In 1991, Higuchi et al. (Higuchi 1991) developed a pocket size EDM system. The authors recognized that drilling hundreds or thousands of holes one at a time was rather inefficient. The pocket-sized EDM system is approximately the size of a pencil, allowing many of the systems to be placed on a large part at the same time, thus drilling several holes at the same time.

In the same vein as the pocket sized machine came the next effort in making micro-EDM more parallel. While some researchers were exploring the use of LIGA-made electrodes to improve the accuracy of EDM, one research group was making an array of posts using the LIGA process (LIGA is a German acronym for lithography, electroplating and injection molding) (Takatata 1999, 2001, 2002). This array of posts could then be sunk into a workpiece using the EDM process to make an array of holes. Again, drilling several holes at once is better than drilling one at a time. An array of 200 holes (20 x 10) was machined in approximately five minutes, 20 to 30 times better than machining the same number of holes one at a time (Takahata 2001). It was found that further improvement in cycle time is achieved if several power supply circuits are linked to the array, thus allowing several sparks to occur at the same time. In fact, using four circuits for an entire array of electrodes, instead of just one circuit for the entire array, cut the machining time in half (Takahata 2002).

The final effort toward increasing the throughput of EDM parts again used an array of posts to make an array of holes in the workpiece. This work, however, used a wire-EDM system to machine an array of square posts into the tool electrode (Weng 2002). This research group found that an array of 49 holes could be machined in 31 minutes, while one hole was machined in 2 minutes. The additional benefit to this process is that wire-EDM is much less expensive than the LIGA process and can produce tool electrodes in a large number of materials the LIGA process cannot.

It is worth noting that each of the research efforts toward improving the throughput of micro-EDM focused only on making the process more parallel, not on actually speeding up or improving the efficiency of the machining process. This, however, should not imply that a parallel process is always better than a serial process. Many parallel processing techniques are very costly and still rather slow, making the serial EDM process a better alternative.

2.1.2 Improving the accuracy or shape complexity of micro-EDMed parts

In the micro-EDM process, tool wear is a major source of inaccuracy. It is possible to choose optimum machining parameters to maximize the ratio of workpiece material removal to tool material removal. But some amount of tool wear is unavoidable. The main methods for overcoming inaccuracies introduced by tool wear are to more precisely position the tool (e.g. Yong 2002) or to better compensate for the wear (e.g. Wolf 1998). One very intriguing method of compensating for tool wear is the so-called “uniform wear method” (Yu 1998-Rajurkar 2000). The main goal of this method is to use only the bottom of the tool (and not the sides of the tool) to do machining, and to machine in such a manner that the electrode remains flat. The uniform wear method is a five-part solution to the tool wear problem. The first aspect of the method is that machining is done layer by layer (much like the opposite of a rapid prototyping machine). The thickness of each layer is determined such that the tool is fully worn at the end of a pass. Once one layer is finished, the tool is sunk down to the next layer, and machining is done in reverse. This is the second aspect of the method: to and from scanning. The tool wears on the “to” pass, meaning the cavity will taper, being deeper at the beginning than at the end. The

solution to this is that the "from" pass machines at the same depth as the "to" pass but in the exact opposite direction. The end result of the two passes is a cavity of equal depth. The third part of the uniform wear method accounts for the fact that the tool has been observed to wear more at its corners than at the center. Overlapping tool paths prevents this. Similarly, when the boundary of a part is being machined, the tool wears unevenly and the edges tend to become round. So machining the central portion of the part and the boundary of the part alternately is the fourth aspect. Finally, an empirical formula to compensate for electrode wear has been determined.

$$\Delta Z = L_w\left(1 + R\frac{S_w}{S_e}\right)$$

R is the electrode volume wear ratio that is specific to each tool/workpiece combination, S_e is the cross-sectional area of the electrode, S_w is the area of the machined layer, ΔZ is the depth of cut, and L_w is the machined depth. These five principles were combined and integrated into a CAD/CAM package to machine some complex and tiny features (Yu 1998, Yu 2000, and Rajurkar 2000).

Another approach to improving the accuracy of micro-EDM is to start with more precise tool electrodes. This is the focus of research done to improve the block electrode method for producing very small cylindrical electrodes (Ravi 2002, Ravi 2002). Using multiple passes and a fresh area of the block lead to more accurately machined tools. It was mentioned earlier that the LIGA process was used to produce tools with multiple electrodes. Actually, that application was a spin-off of the attempt to use LIGA to produce more accurate tools (Ehrfeld 1996, Lowe 1997, Takahata 2000).

Tool wear is not the only aspect of micro-EDM that influences part accuracy or complexity. A major area of concern when machining a very small part is that the part is easily lost at release or separation. Because of this, many micro-parts are not truly three-dimensional; they are considered 2.5D. One research group has successfully produced a truly three-dimensional part in silicon using only the micro-EDM process (Reynaerts 1998).

One might note that these efforts in improving the accuracy of micro-EDM often trade off other aspects of the process. While LIGA does produce more accurate electrodes, it does so rather expensively. The main drawback of the uniform wear method is that it adds a significant amount of time to the already slow micro-EDM process. The cavities machined in the research were done in hours, not minutes. However, it should be noted that all of the methods mentioned above can be incorporated into the experimental setup of the present study.

2.1.3 Novel applications of micro-EDM

Another topic popular with micro-EDM researchers is increasing the number of tasks micro-EDM is used to accomplish. Some papers compare micro-EDM to other micro- and meso-scale machining processes, expounding on the low forces of micro-EDM and its small unit removal (Masuzawa 1994, Allen 2000, Allen 2000 again). Others investigate new materials micro-EDM can machine (Reynaerts 1997, Heeren 1997, Yan 2002). Finally, some just find new applications for micro-EDM, like micromachining with Tungsten Carbide (Her 2001), nozzle hole fabrication, machining gear trains (Shibaike 2000), photomasks (Yeo 2001), and forming tools (Uhlmann 1999). Again, any improvements to the micro-EDM process found in the present study, or any study for that matter, would benefit these applications.

2.2 Existing Micro-EDM Systems

While die-sinking and wire-EDM systems have been around for some time, micro-EDM systems are rather new to the EDM industry. One researcher mentions the pioneering of micro-EDM goes back as far as the 1960s at Phillips Lab in the Netherlands (Reynaerts 1997). However, no documentation on the specifics or capabilities of the mentioned machine could be obtained. After this research was lost, micro-EDM started to evolve purely in the field of small-hole making (Kagaya 1986, Sato 1986, and Masuzawa 1989). While small steps were taken at improving these hole-drilling machines, a major step was taken toward improving micro-EDM as a process with the advent of wire-electro discharge grinding, or WEDG (Masuzawa 1985, 1986). The WEDG process is used to make very small, precise shafts, examples of which can be seen in the citations (Masaki 1990). While there were several applications that benefited from the use of these shafts (Masuzawa 1994), the application that benefited the most was micro-EDM

itself. When the idea to use the WEDG manufactured shafts as micro-EDM tool electrodes, present day micro-EDM was born. Today the best micro-EDM systems create their own tool electrodes directly on the machine utilizing the WEDG technique. The tool electrode is then moved over to machine tiny holes or complex shapes into the workpiece.

Presently, there are only three manufacturers selling micro-EDM systems while other companies are marketing larger "macro" EDM systems, designed originally for large volume removal, that have been adapted to machine very small parts. Panasonic Factory Automation (a division of Matsushita Electric Corporation of America, Illinois, USA, www.panasonicfa.com) makes an MG-ED82W. Sarix SA (Losone, Switzerland, www.sarix.com) makes the SR-VHPM. Pacific Controls Inc. (California, USA, www.pacificcontrols.com) makes the PC SFF Series EDM system. These are the most precise machines available from each company. Key capabilities of each machine are discussed below, and are summarized in Table 2.1. Major manufacturers of die-sinking and wire-EDM systems have also tried to enter the micro-EDM market. These companies do so by equipping their macro-EDM systems with precision positioning stages or micro-generator power supplies. One machine that fit this description was the Charmilles HO-10 (Almond 1999), however, this machine is no longer on the market, so very little information concerning the machine could be obtained. Agie SA (Losone, Switzerland, www.agieus.com) makes two such machines. The Agie Compact I is a die-sinking machine with a micro-generator and more precise positioning than its macro-EDM counterpart. This machine is much older and less precise than the Agiecut Excellence 2F, which is a wire-EDM system that has very precise machining stages and is capable of cutting with 25μm diameter, tungsten wire. The capabilities of this machine are also shown in Table 2.1.

Based on the specifications and the examples shown, the Panasonic machine is clearly the best of the lot. It is the Panasonic system that utilizes WEDG technique to produce tool electrodes directly on the machine. This process is capable of producing electrodes small enough to bore 5μm diameter holes. Additionally, this machine is capable of machining in each of the x-, y-, and z-axes. This allows complex shapes, like gears, to be machined accurately with a generic, cylindrical electrode. The power supply for this machine is a very simple RC circuit that is capable of producing pulses as short as 10 nano-seconds. These very short discharges are ideal

for removing small, precise volumes of material at a very high rate. Much of the research mentioned previously in this chapter, especially the uniform wear work, utilized this type of Panasonic machine.

Table 2.1. Commercially available micro-EDM systems and their capabilities.

Machine	Power Supply	Motion Control	Electrode Size	User Applications
Panasonic	Relaxation Generator (RC circuit) 10 nsec pulse-width	0.1 µm resolution 1 µm positioning accuracy	Holes as small as 5 µm, WEDG makes electrodes on machine	Three axis machining and WEDG allow gears, shafts, etc as well as holes and complex cavities. Real 3D shapes.
Sarix	Undisclosed 50 nsec pulse-width 0.05 – 40 amp	1 µm resolution 1 µm positioning accuracy	Electrodes as small as 12 µm diameter (purchased)	Holes. Shaped electrodes make shaped holes. Machining in 3 axes possible, but not demonstrated.
Pacific Controls	555 multi-shot (dual gap voltage) 2.5 µsec pulse-width 0.002 – 100 amp	Monitored to 0.5 µm	Electrodes as small as 2.5 µm diameter (purchased)	Holes only, no mention of shaped electrodes. Machining only in z-axis
Agie	Undisclosed	0.1 µm resolution 1 µm positioning accuracy	Wire as small as 25 µm diameter (purchased)	Any type of 2-D part. Machining in x- and y-axes only. Wire tilt not available with 25µm wire.

Sarix and PCEDM offer machines that are capable of machining on the micron level, but are not nearly as robust as the Panasonic machine. Sarix claims that their system can cut in all three axes, but the examples mentioned in their literature are only of hole making. This system is capable of cutting very small holes and complex shaped holes with shaped electrodes. However, shaped electrodes dramatically increase costs and time associated with tooling. The company was unwilling to share the type of circuit they use to produce pulses, but the smallest pulse achievable is not as small as the 10 nano-second pulses by the Panasonic machine. PCEDM is a relative newcomer to the market, and not much is known about the company or its machines. They were, however, very willing, almost eager, to discuss the details of their machine. Similar to the other machines, the SFF series machine can cut very tiny holes, and can do so rather quickly. However, hole making is the only application the machine can accomplish as it only machines in the z-direction. The x and y positioning are very precise on this machine, but not capable of correcting for open and short circuits, and will almost certainly result in broken tools

if machining were attempted. Additionally, the use of a 555 multi-shot chip as the main pulse modulator is a rather archaic technology.

The Agie machine compares reasonably well to the other micro-EDM systems, keeping in mind that it is a wire-EDM system where as the other machines are hybrids of die-sinkers. The x and y stages on the Agiecut, the stages responsible for machining, are as accurate or more accurate than the machining axes of the other micro-EDM systems. However, the tool electrode size on the Agie system is really a limiting factor. The 25μm wire is about as small a tool that can be used for cutting, and this wire was relatively difficult to work with. It is highly unlikely that wire as small as 5 microns could ever be used on this type of machine. However, it is important to remember that the Agiecut is a macro-, wire-EDM system. One could argue that this is a comparison of apples and oranges. It might be more informative, or more fair, to benchmark the Agiecut against other macro-EDM systems adapted to perform micromachining. However, these are often custom or in-house modifications and would be rather difficult to find.

When asked about motion control, each company replied with how accurate their machines were, leaving out important information on how the machine compensates for open and short circuits and for tool electrode wear. When the stages are moving faster or slower than material is being removed, short or open circuits, where no material removal occurs, will inevitably result. It is desirable that the stages compensate for this, maintaining a constant amount of material removal. Also, as the tool cuts, it too is eroded to some extent, although at a slower rate than the workpiece. Because of this, over time, the electrode will be smaller, or at least a different shape, than when machining started. If the machine cannot compensate for this, dimensional accuracy will be lost. It may very well be that these companies recognize the importance of this aspect of motion control and would like their technology to remain secret. However, this fact makes it rather difficult to compare machines against each other.

Despite the quality and potential of these micro-EDM systems, only one of seven EDM job shops that replied to a market survey uses one of them as part of its operation. An internet search on micro-EDM job shops yielded several locations within the U.S. Each of these shops was contacted via business letter. Seven of those contacted replied. Only one of the seven was

devoted exclusively to micro-EDM jobs, the same operation that owned a Panasonic micro-EDM system. The remaining six did micro-EDM jobs in addition to large-scale wire-EDM and/or die-sinking EDM. These job shops were working on a variety of jobs for a variety of different customers. However, almost all of the jobs had at least one thing in common; they were prototype jobs. Only one operation had any type of production job, and because of privacy issues, could not discuss the details of the job. Additionally, the vast majority (~ 85%) of micro-EDM jobs performed were purely hole making jobs. This survey, while by no means exhaustive, illustrates the fact that micro-EDM systems, and the process as a whole, are rarely being used to their full potential. Other companies that have purchased micro-EDM systems of their own (and do not need to contract job shops to get the work done) may better use their systems' capabilities. However, finding out which companies have purchased these machines, then contacting them and getting information on how they use their machines would be difficult.

2.3 Benchmarking Experiments

The Agiecut Excellence 2F mentioned in the previous section was available for benchmarking experiments courtesy of center 14184 of Sandia National Laboratories in Albuquerque, New Mexico, USA. The main question to answer was, "How small of a feature can the Agie machine cut?" A test part was designed to help answer this question, and the part was cut several times using several machine parameters resulting in similar degrees of success. The part was essentially a 6mm x 5mm rectangle with progressively smaller tabs protruding from the long side of the part (see Fig. 2.1). The largest tab was 30μm wide, and the smallest tab was 2μm wide. All tabs were 100μm long, and were separated by 1mm. The material used was 100μm thick stainless steel. The Agie's control software recommended parameters that were used for the first several cuts. Using these parameters, the part was cut in approximately 12 minutes, and the smallest tab observed on an optical gauging machine was 20μm wide. The disappointing part of this test was that the tab observed to be 20μm was intended to be only 15μm. Indeed, all the tabs present on this test part were cut approximately 5μm too wide, yet other dimensions (tab length and spacing) were hit exactly. Most of the other machine settings produced very similar results. However, it was found that slowing the machine down resulted in more accurate tabs. When the machine was set to cut the part in 30 minutes (the pulse time delay was increased by 50% from

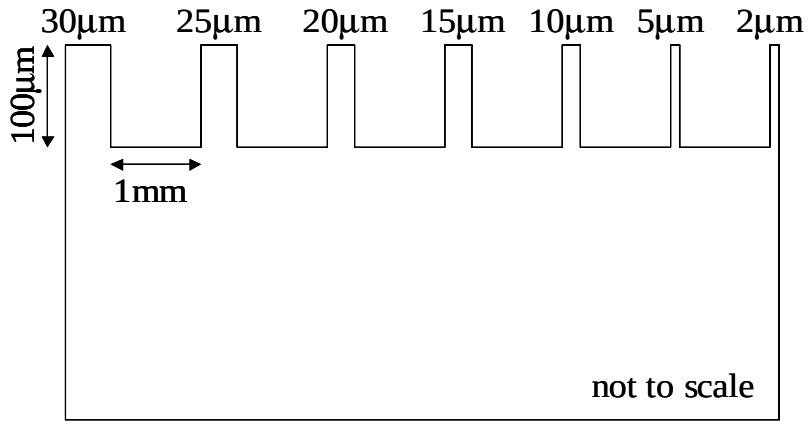

Figure 2.1. Schematic of the test part designed to evaluate the smallest feature size attainable by the Agiecut Excellence 2F.

50 to 75), the tabs were only 1 to 2µm too wide. However, the smallest tab still measured 20µm in width (Fig. 2.2).

The feature shown in Fig. 2.2 is a male feature, or a feature external to the main geometry. The minimum size of such features is governed primarily by the accuracy of the machining axes. The size of the tool and the overburn of the cut govern a minimum size of a female feature, for example a slot or a cut internal to the geometry. For the Agie machine, the smallest tool that can be used is 25µm diameter wire and the smallest overburn was observed to be 12µm. This means that the smallest slot machined by the Agie machine was 50µm. It should also be noted that minimum feature sizes could be dependent on the workpiece material and the workpiece thickness, but those effects are considered secondary.

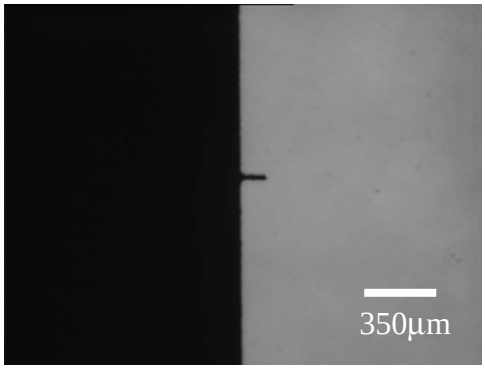

Fig. 2.2. An optical micrograph showing the 100µm long, 20µm wide tab cut using a time delay of 75.

3. Experimental Setup

The main focus of this project is the novel experimental setup and its performance, studying machining rates and feature sizes. The entire setup, shown in Fig. 3.1, constitutes five main areas: motion control, power supply, tool and workpiece fixturing, analysis systems, and dielectric unit. The dielectric, tool and workpiece reside in the machining vessel, and are connected to the analysis tools (a digital oscilloscope and personal computer), but what makes the setup unique is its use of a dual-level servo system, comprised of a linear stage and piezoelectric actuator, for motion control and a transistor-based pulse power supply. This should not imply that the other aspects of the micro-EDM process are of any less importance. However, since a main focus of the experiments is on the influence of the power supply and motion control, solutions to the peripheral aspects of micro-EDM were very simple, so as not to influence the results. Improved solutions for these peripheral aspects will still be compatible with the new motion system and power supply and will only improve the process. The simple solutions to tooling, dielectric unit, and measurement are summarized in this chapter's third section. The first two sections discuss the details of EDM power supplies and motion control units, and how the solutions proposed in this study are improvements over the current leading technologies.

3.1 Purdue Pulse Power Supply

A power supply or pulse modulator for traditional EDM processes creates square voltage pulses of a specified width (duration), open-circuit voltage, and frequency (ref. Fig. 3.2a). Each pulse results in one of four types of discharges. One discharge is actually not a discharge, at all; it is an open circuit where the tool electrode is too far away from the workpiece electrode for a discharge to occur. In this case, the gap voltage looks exactly like the power supply's voltage pulse, and no current flows. A second type of discharge is a "short", occurring when the tool is in direct contact with the workpiece. In this case, the gap voltage registers as zero while a current constantly flows. A third type of discharge is classified as an "arc". An arc is characterized by current flowing between the tool electrode and workpiece electrode immediately upon initiation of the power supply pulse, and the gap voltage never reaching its

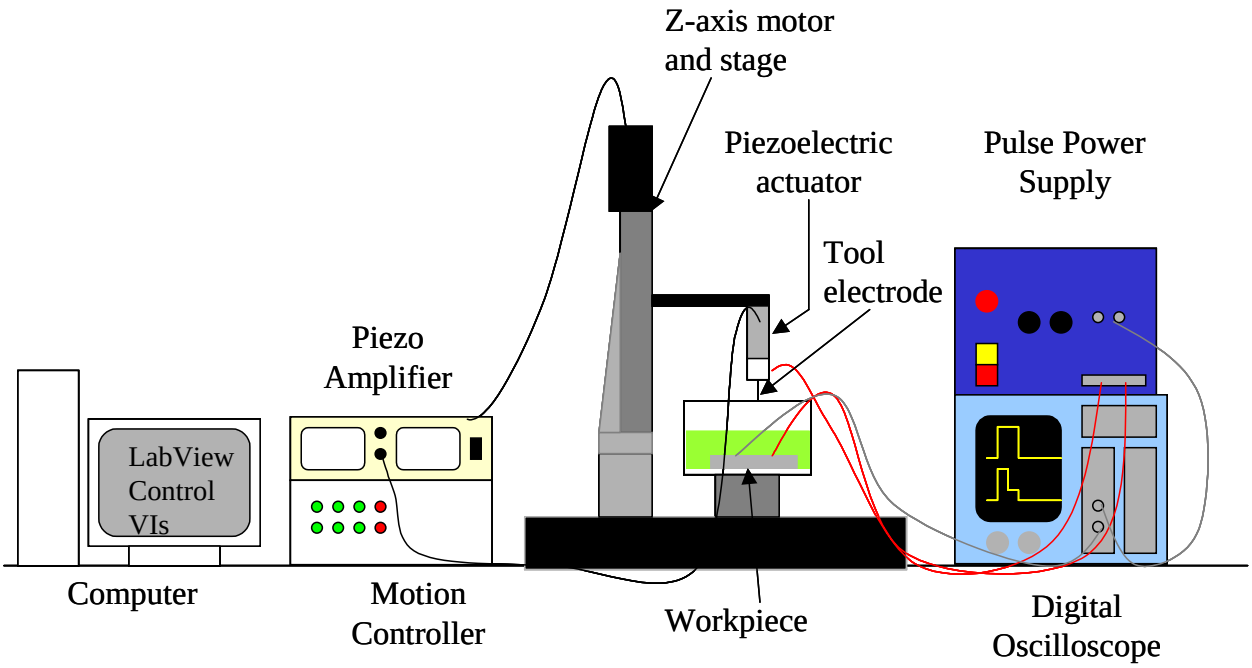

Figure 3.1. Schematic of the entire micro-EDM setup used in the present study. The unique aspects of this setup are the pulse power supply and the dual-level servo system comprised of the z-axis stage and the piezoelectric actuator.

open circuit value. All three of these discharges are considered "bad" discharges in that they adversely affect the machining efficiency or decrease material removal rates (Barash 1964). A good discharge, or "spark", involves the gap voltage rising up to its open circuit value until, after a time delay, a discharge is established and current flows. At this point, the current rises to a maximum value, and the voltage drops to the discharge voltage, and remains constant until the power supply switches the pulse off. These four types of discharges can be seen in Figs. 3.3 and 3.4. A schematic of a spark discharge can be seen in Fig. 3.2.

A main difference between die-sinking EDM, wire-EDM, and micro-EDM is the width of the voltage pulses. As can be seen in Figs. 3.3 and 3.4, the pulse-widths in die-sinking EDM are a few hundred microseconds. In wire-EDM, pulse-widths tend to be in the tens of microseconds range, while micro-EDM often uses pulse widths as small as only 50 nanoseconds. Spur (1990) addresses the fact that wire-EDM's voltage pulses are faster

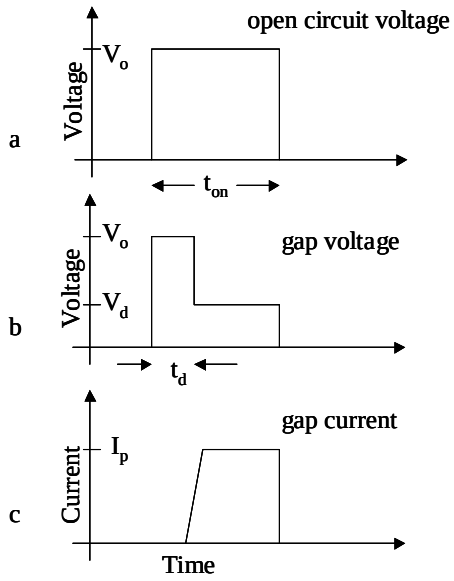

Figure 3.2. Schematic illustrating the event sequence involved in creating a discharge with a pulse power supply. Vo = open-circuit voltage, Vd = discharge voltage, Ip = peak current, ton = voltage pulse-width, and td = time delay. Inputs are typically Vo, Ip, and ton while other values vary somewhat from discharge to discharge.

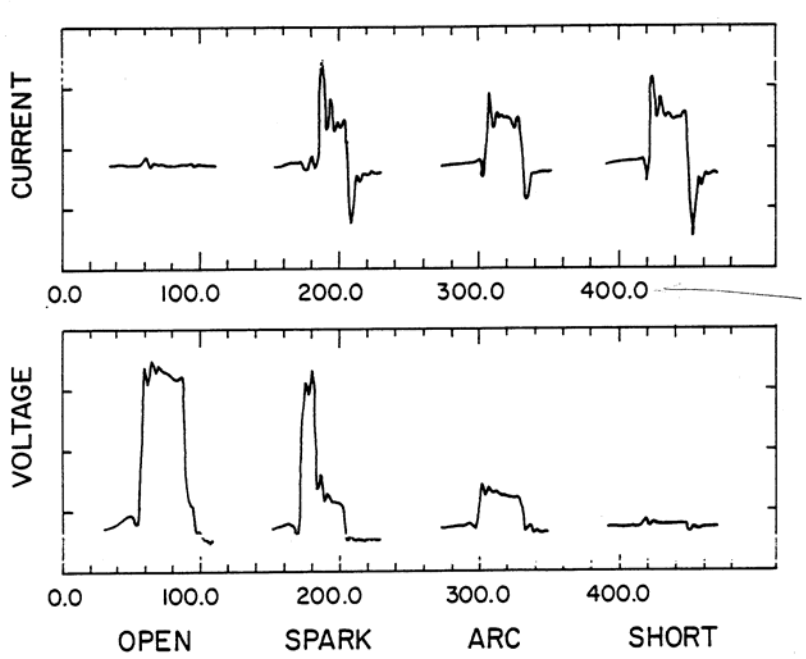

Figure 3.3. The gap current and gap voltage for the four types of discharges seen in the EDM process. Only the "spark" discharge is considered a good discharge. (Rajurkar 1987).

and mentions that while gap voltage waveforms look similar to die-sinking-EDM gap voltages,

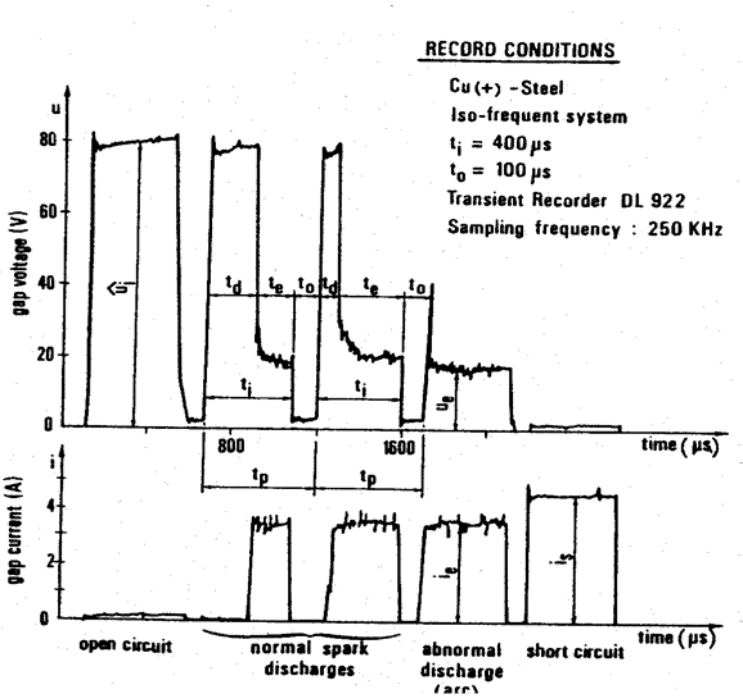

Figure 3.4. Waveforms typical of the four types of EDM discharges. (Snoeys 1982).

the gap current in wire-EDM may never reach a steady-state value. Figure 3.5 shows a schematic of typical wire-EDM gap voltage and current waveforms.

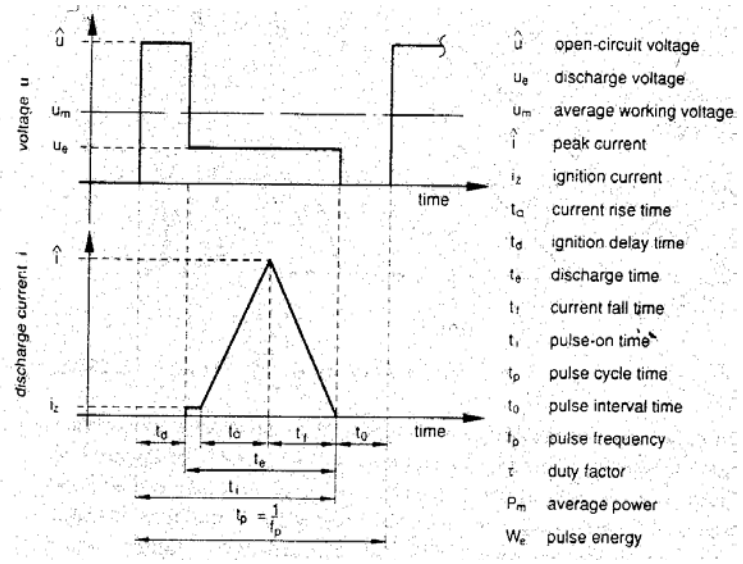

Figure 3.5. Schematic illustrating a typical wire-EDM discharge with important values labeled. (Spur 1993).

Often, transistors or multivibrator integrated circuits are used to generate the square pulses for die-sinking and wire-EDM. These solutions are not fast enough to create pulses on the order of nanoseconds as desired in micro-EDM. Micro-EDM typically relies on DC voltage supply through RC circuits to create square pulses. For this type of circuit, the discharge event sequence is different than that of the pulse modulator described earlier. Since a DC voltage is employed, the normal operating condition is at the open-circuit voltage, so the electrodes are always charged. The two electrodes are then brought close enough together to breakdown the dielectric. At this point a discharge commences; the voltage drops to the discharge voltage and the current rises to its peak. Current continues to flow until all the energy is drawn out of the capacitor, at which time the current stops and the voltage recharges to the open-circuit voltage (see Fig. 3.6). The next discharge occurs when the electrodes again are close enough to breakdown the dielectric.

When using a DC voltage source and an RC circuit to produce pulses, the only controlled inputs are open-circuit voltage and pulse-width. The pulse-width is varied by changing the capacitance in the circuit. There is no real control over discharge frequency because the only determining factor is electrode proximity, and discharges occur much more quickly than the tool can be positioned.

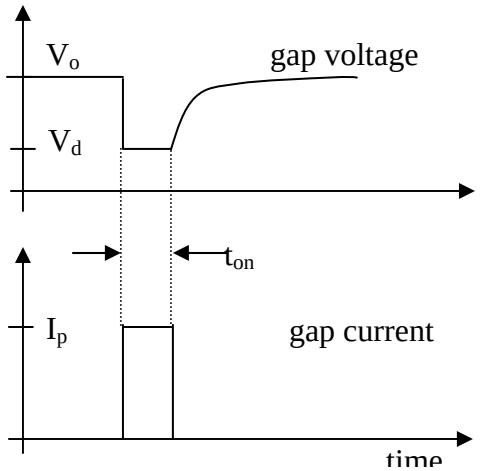

Figure 3.6. Schematic illustrating the event sequence of a discharge created using DC voltage through an RC circuit. V_o is open-circuit voltage, V_d is discharge voltage, I_p is peak current, and ton is pulse-width. V_o and t_{on} are the controlled variables.

The pulse modulators for die-sinking and wire-EDM are superior from a control standpoint because discharge frequency can be regulated. Since a discharge can only occur if the electrodes are close enough AND a pulse has been sent from the power supply, frequency is controlled by controlling when the power supply sends pulses. This added level of control allows for better monitoring of the process and more influence over process performance. However, existing EDM pulse modulators are not nearly fast enough to compete with the RC circuits.

One of the goals of this project was to utilize a power supply that would allow for enhanced control over the micro-EDM process, thus control of frequency and duty-cycle were desired. To accomplish this, a pulse-modulator that creates square voltage pulses by switching a transistor on and off was custom built.

What was desired of the micro-EDM pulse power supply was a device that could produce voltage pulses with a very short pulse-widths (as small as 100nsec) and open-circuit voltages as high as 300 Volts. The pulses would need to be able to draw as much as 10 Amperes in current. Control over pulse frequency and duty-cycle were also desired. Additionally, in order to conduct experiments, all of the above parameters needed to be variable. Based on these design specifications, North Star Research Corporation (New Mexico, USA, www.northstar-research.com) developed a power supply for micro-EDM—the Purdue Pulse Power Supply. Circuit diagrams in the appendix show the specifics of the power supply, and its performance specifications are summarized in Table 3.1. The supply is able to produce pulses with pulse-widths of 100nsec and upwards. The open-circuit voltage is continuously variable from 0 to 300V. The peak current drawn by the discharge has settings of, 0.01A, 0.1A, 0.5A, 1A, 2A, 5A, 10A, and full current. A computer control program that controls a fiber optic switch is used to set the pulse-width and pulse frequency. Almost any frequency can be set for any desired pulse-width, allowing for unlimited duty cycle settings. The main switching mechanism that allows such short pulses with fast rise times is an insulated gate bipolar transistor (IGBT). The IGBT is a recent invention that combines the simple gate drive characteristics of the MOSFET with the high current and low saturation voltage of bipolar transistors, and is mainly used in switching power supplies (www.nationmaster.com/encyclopedia/IGBT-transistor).

Table 3.1: Available machining settings using Purdue pulse power supply.

Power Supply Setting	Realizable Conditions	Settings used in experiments
Output Voltage (V_o)	0V to 300V	100V and 200V
Peak Current (I_p)	0.01A to 10A	1A
Pulse Width (t_{on})	100nsec to 100μsec	500nsec and 1μsec
Frequency (f)	0.1Hz to 10MHz	10kHz and 20kHz
Duty Cycle	any	1:100

3.1.1 Characterization of Purdue Pulse Power Supply performance

The Purdue Pulse Power Supply produced open-circuit voltage pulses that accurately reflected the inputs of open-circuit voltage, pulse-width, and pulse frequency (or duty cycle). An example is shown in Fig. 3.7a. However, when the tool electrode and the workpiece come in close enough proximity to produce a discharge, the gap voltage and current did not behave as expected. The process starts predictably when the gap voltage rises to the open circuit voltage and remains there for some time delay. After this delay, when the discharge commences, the current rises and the voltage drops to the discharge voltage. To this point there are no problems. However, the current usually rises to a value other than the peak current input. Once the current does reach its maximum, it immediately starts decreasing. The current continues to decrease at a certain rate until it is zero. An example set of waveforms is shown in Fig. 3.7.

The waveforms in Fig. 3.7 are from a discharge with 100V, 1A, and 1µsec settings for open

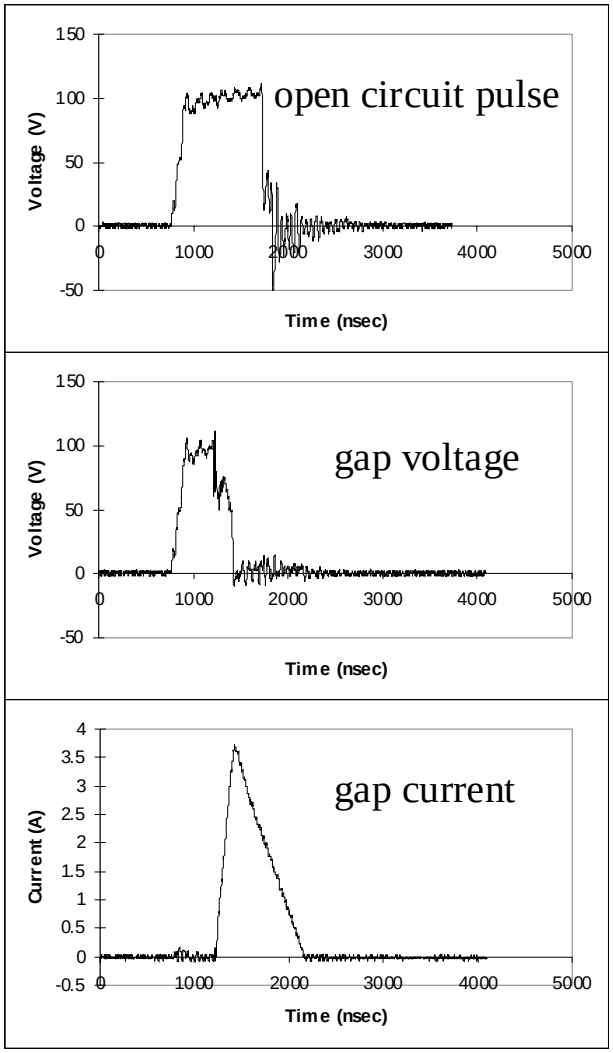

Figure 3.7. The Purdue pulse power supply produced discharges that had waveforms typical of the ones shown in the figure. Inputs: open-circuit voltage = 100V, pulse-width = 1µsec, peak current = 1A.

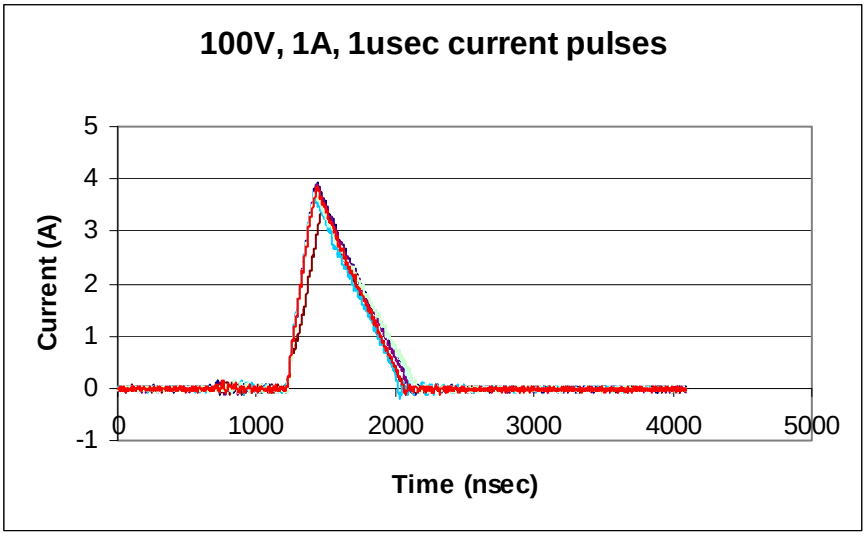

Figure 3.8. Fourteen current traces are overlaid. Inputs: V0 = 100V, ton = 1µsec, Ip = 1A. These traces indicate the consistency of the PPPS.

circuit voltage, peak current, and voltage pulse-width respectively. Fourteen of these waveforms were captured and compared for repeatability. Figure 3.8 shows all fourteen current waveforms overlaid on top of one another. This plot indicates that while the peak values are larger than the peak current setting, the current waveforms are very consistent. At the given settings, the peak current is approximately 3.8A and has duration of approximately 900nsec. When the open circuit pulse was increased in duration to 2µsec a similar occurrence was observed. The current waveforms rose to peaks of 4.2A and had durations of 1100 nsec and were, again, consistently the same.

Another characterization experiment was performed in which the peak current setting was changed. Peak current inputs of 1A, 2A, 5A, and 10A were examined with an open-circuit voltage setting of 100V and duration of 1μsec. The majority of the current waveforms resembled the waveform shown in Fig 3.7 with the exception of an increase in peak current value and an increase in current duration as the peak current setting increased. Again, the peak current setting did not correspond to the measured peak current value. Typical current waveforms from each peak current setting were overlaid for comparison (Fig. 3.9). This figure shows that the rise of the current toward its peak value occurs at the same rate (i.e. the waveforms have the same slope). The current waveforms also all fall toward zero at the same rate. However, the rise rate is not equal to the fall rate.

Changing the open circuit voltage seems to have the most drastic effect on the resulting current waveform. When the open circuit voltage was changed to 200V (the pulse-width setting was 1μsec and the peak current setting was 1A) the current rose to a higher peak current value more quickly. Doubling the open circuit voltage created a 58% increase in measured peak current (3.8A to 6.0A), while doubling the peak current setting only produced an increase of 26% (3.8A to 4.8A) and doubling the open circuit pulse duration resulted in only an 11% increase (3.8A to

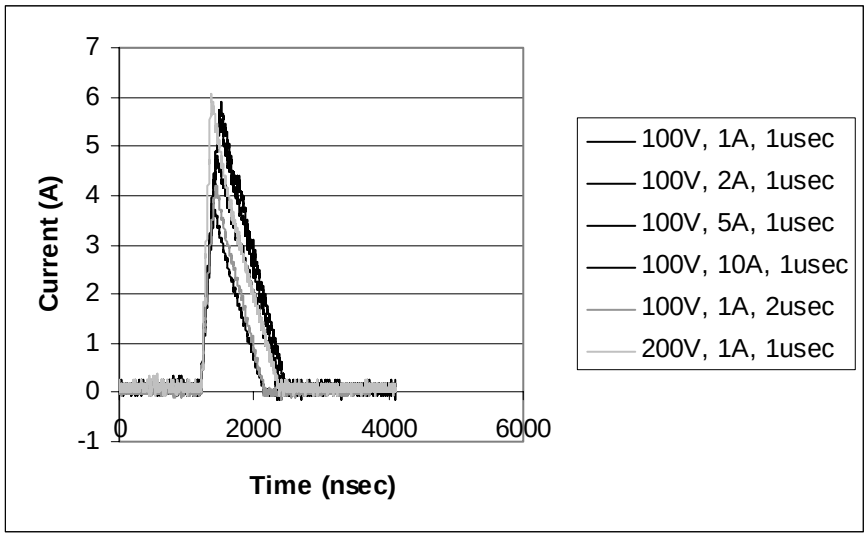

Figure 3.9. Current waveforms from various discharges overlain. The waveforms appear to have the same rise rate and fall rate if the open-circuit voltage setting is the same. Peak current value and pulse-width increase with increasing peak current setting.

4.2A).

In conclusion, the current pulse duration is a function of the rise rate, the observed peak current, and the fall rate. These three values are very consistent for a given set of inputs, but their values do not correspond to those inputs. Put more simply, the current waveforms resulting from a pulse with inputs of 100V, 1A, and 2μsec look the same, but the peak current is 4.2A (not 1A) and has duration of 1.2μsec (not 2μsec). While the observed peak current varies with all three inputs, the rise rate and fall rate appear to change only with changes in the open-circuit voltage. Since the square, open circuit voltage, gap voltage, and gap current waveforms are all very consistent, controllable, and easily calibrated, the Purdue pulse power supply is more than adequate for the proposed experiments.

3.1.2 An alternative power supply

Pulse forming transmission lines (PFL) can be used to generate electrical discharges. The most common form of transmission line, a coaxial cable, provided alternative to the Purdue Pulse Power Supply. The cable was semi-rigid copper, with a characteristic impedance of 50Ω and capacitance of 30pF/ft. Each cable was only five feet long, but several could be connected together using standard SMA connectors for a maximum length of 65 feet. Combining the resistance and capacitance of the coaxial cable with a DC power supply and a charging resistor results in an RC circuit similar to those used in typical micro-EDM systems (like the relaxation circuit in the Panasonic system). The benefit of the PFL used in this study is that a switch can be added ahead of the coaxial cable allowing the circuit to discharge only once without recharging (see Fig. 3.10). This means that examining the results (crater size and morphology) of a single micro-EDM discharge is fairly simple.

The widths of the pulses formed by this circuit are given by the transit time, τ, of the transmission line

$$\tau = \sqrt{LC} = x\frac{\sqrt{\varepsilon_r}}{c}$$

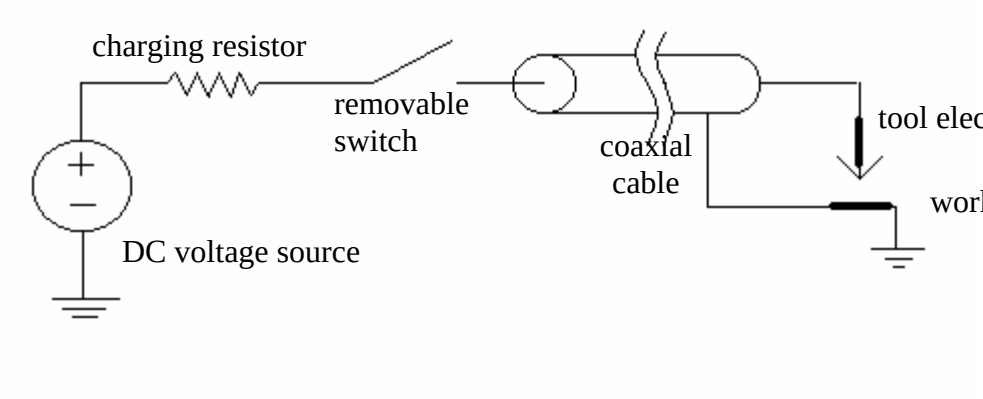

Figure 3.10. Schematic of the transmission line circuit used as an alternative power supply.

(*L*, inductance, *C* capacitance, x, length of cable, ε_r, cable dielectric coefficient, and *c*, the speed of light in vacuum). It is important to note that τ (along with capacitance) varies with the length of cable, which allows the pulse-width to be varied simply by changing the length of cable. In the present setup, τ is ~3 nsec per foot of cable length. A sample current pulse resulting from a cable length of 65ft and a DC power supply setting of 150V is shown in Fig. 3.11. Even though this power supply is capable of producing pulses with smaller pulse-widths than the Purdue Pulse Power Supply, it is viewed as inferior because there is no control over discharge frequency.

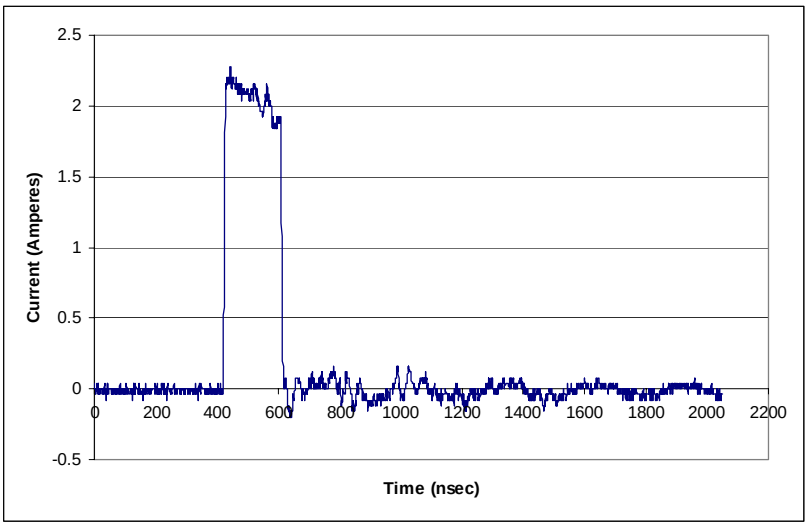

Figure 3.11. Sample current waveform from a discharge produced with the alternative power supply shown in Fig. 3.10.

3.2 Motion Control

The EDM process is demanding of its motion control system, which is used to position the electrodes. If the tool electrode advances too slowly, the process is very inefficient since many pulses sent from the pulse power supply result in no discharge, and therefore no material removal. If the servo advances too quickly, a short circuit results, again with no material removal, but also with the risk of welding the tool to the workpiece. The depth of material removed by a single discharge of micro-EDM is typically less than 5μm, and discharges occur at frequencies as high as 100kHz. Additionally, debris created by the removal process often floats around in the spark gap area, creating short circuits or bad discharges. Ideally, the servo system should be able to respond to the result of every discharge, or at least on the same order as the discharge frequency to minimize the number of bad discharges. There should be no overshoot when the servo is advancing since additional short circuits might result. It should also be able to advance at speeds and steps on the order of the amount of material being removed. The result of all this is a rather contradictory requirement—slow long-range movement along with quick, precise short-scale movement.

The motion system that best meets these requirements is a patented hybrid servomechanism composed of two devices, a fast, easily controllable, short stroke actuator for good "instantaneous" response, and a slower actuator for positioning the fast actuator and for providing the required long stroke (Hebbar 2002). Such a hybrid system allows the slower actuator to feed the tool electrode into the workpiece utilizing its long stroke, and the fast, short stroke actuator to respond quickly to instantaneous variations in the spark gap conditions. For the purposes of this experimental setup, the fast, short stroke actuator is a piezo-electric actuator and the slow, long stroke actuator is a motorized, linear translation stage.

Newport Corporation's (California, USA, www.newport.com) MTM250CC.1 long travel linear stage is very well suited to the demands of the micro-EDM experimental setup. The small removal rates, and therefore low feed rates, of micro-EDM demand smooth and precise movement from the long-stroke actuator. The MTM250CC.1 (hereafter referred to as the z-stage) utilizes a servomotor driver geared down to allow positioning with 0.1μm resolution. The

DC servomotor is connected to the linear slide by a diamond-corrected lead screw and a matched, anti-backlash, precision-lapped nut. The stage is of all-steel construction, making it very stiff, and allowing it to bear an axial load of up to 100 N. A Newport motion controller, the MM4006, is used to drive the z-stage based on LabVIEW programs written on a PC.

The advantages of a piezoelectric actuator are that it has a very fast response of less than 10μsec with high accuracy, and simple, stable control. The Physik Instrumente (Waldbronn, Germany, www.physikintrumente.com) P-844.30 preloaded piezoelectric translator (hereafter referred to as the PZT) proved quite suitable for this application. The spring preload allowed the PZT to transmit forces as high as 100N. Both the tip and the base were threaded allowing for easy fixturing of the PZT to the z-stage. The PZT required an amplifier (BOS 100-4 by Lambda EMI, Inc., New Jersey, USA, www.lambda-emi.com) that boosted an input voltage by ten.

The tool electrode was held by a simple tool holder specifically designed to the present application. The top of the tool holder has a threaded hole, allowing the tool holder (and thereby the tool) to be screwed directly onto the tip of the PZT. The top of the PZT is bolted to a connecting arm, the other end of which bolts to the linear slide of the z-stage. The z-stage is held vertical by a Newport vertical mounting bracket. This bracket is connected, at the base, to a vertical standoff (to position the stage at the proper height), which is further connected to the base of the entire setup. A schematic, Fig. 3.12, illustrates the entire motion control system.

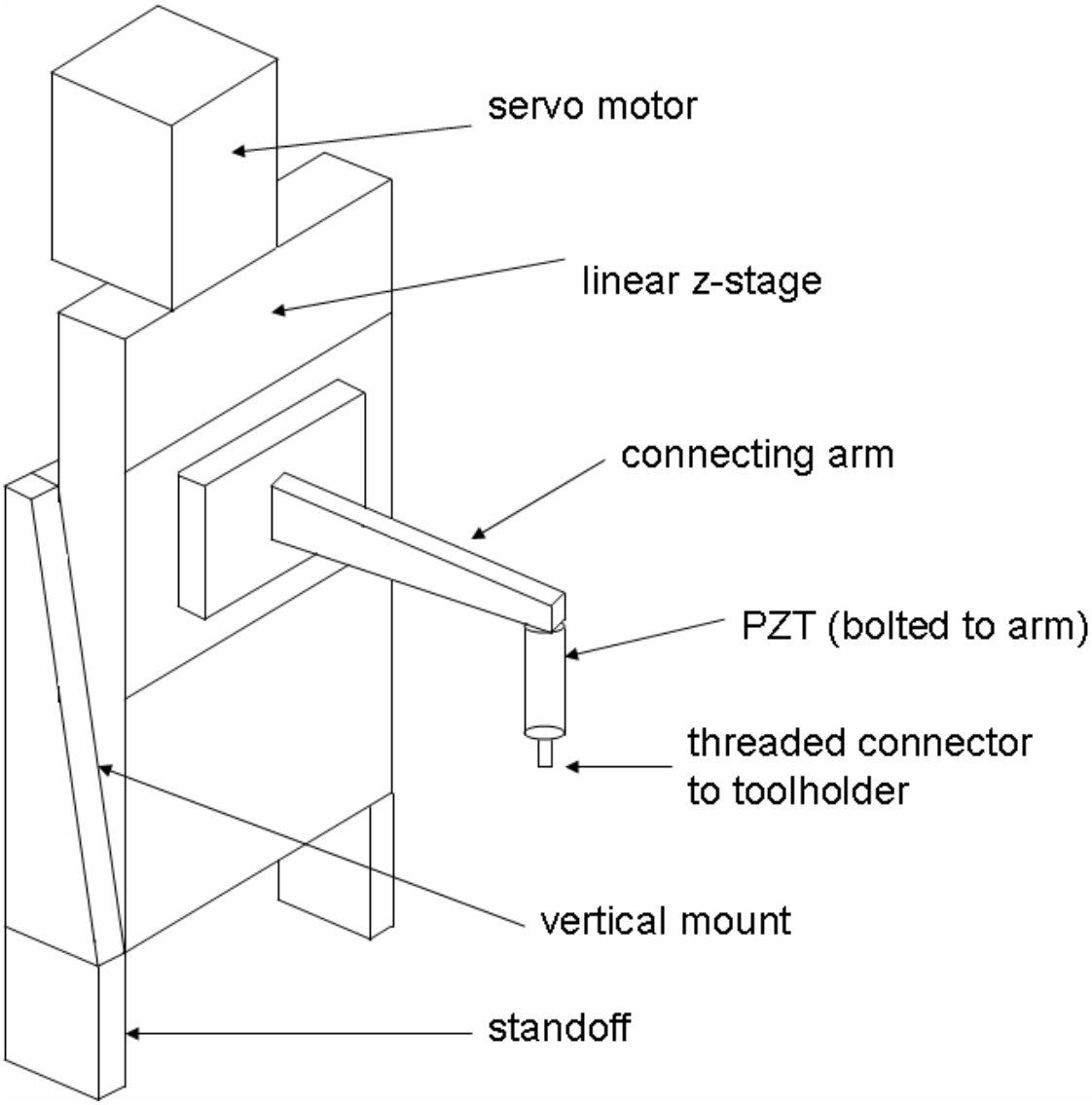

Figure 3.12. A schematic illustrating the entire motion control system.

3.2.1 Control of motion system

There are many methods of control available for the PZT, the best of which would stem directly from gap conditions. At a minimum, a wave function generator can be used to vibrate the tool electrode with a sine wave or square wave input. This vibration prevents the tool from welding to the workpiece during machining and allows for dielectric liquid to flow into the machining area more easily, overcoming two problems usually encountered while feeding the electrode with only the z-stage. However, monitoring the gap conditions, and changing the PZT input accordingly will help improve the machining process. Reacting to each and every discharge is

ideal, but discharges may be occurring at a frequency too high to make this practical. Using some sort of averaged gap conditions to position the PZT is a more likely control scenario.

LabVIEW control programs were written to operate the z-stage for preliminary experiments in single discharges of micro-EDM and in hole-making. For the single discharge experiments, LabVIEW was used to run both the z-stage and an oscilloscope via GPIB. The z-stage fed down, moving the tool closer to the workpiece, until the oscilloscope triggered, registering the discharge and recording the voltage and current pulses across the machining gap. When the oscilloscope triggered, a command was sent to the z-stage to stop and retract. Hole making is a much more complicated process because the z-stage needs to feed while discharges are occurring. For the preliminary experiments, open loop control was used. The PZT was set to oscillate at a constant applied voltage and frequency. The z-stage was set to feed at a constant rate. If the feed was too slow, resulting in long periods of open circuit, nothing was changed except that a higher feed rate was used in subsequent tests. However, short circuits posed a serious problem. To address this, a "short retract" button was included in the LabVIEW control program. The oscilloscope was set to acquire gap voltage and current conditions continuously, so that a short circuit would register as zero voltage between the tool and workpiece. When the operator noticed this, the "short retract" button was depressed and commands were sent to the z-stage instructing it to stop and retract by 5μm. After this retract was completed, the z-stage was allowed to continue feeding the tool toward the workpiece at the feed rate specified.

3.2.2 Calibration of motion control devices

Calibration of the PZT was done by inputting various types of signals and measuring the motion of the PZT with a capacitance probe. Peak-to-peak voltage waves of 1V, 3V, and 9V were sent from a frequency generator through the amplifier and to the PZT at frequencies of 50Hz and 100Hz (unfortunately, the capacitance probe is limited to measuring movements of 200Hz or slower). Both sine waves and square waves were investigated. The data from the capacitance probe were analyzed, many cycles were averaged, and the amplitudes of the PZT translations were computed. The results of these tests are shown in the Table 3.2 and typical cycle traces are shown in Fig. 3.13.

Table 3.2: Peak-to-Peak amplitudes of PZT resulting from a sine wave input (left) and a square wave input (right). All standard deviation, coincidentally, are 0.3 μm.

	50Hz	100Hz			50Hz	100Hz
1V	3.0μm	2.8μm		**1V**	4.4μm	3.7μm
3V	8.0μm	6.0μm		**3V**	11.5μm	4.0μm
9V	39.0μm	38.5μm		**9V**	58.5μm	51.5μm

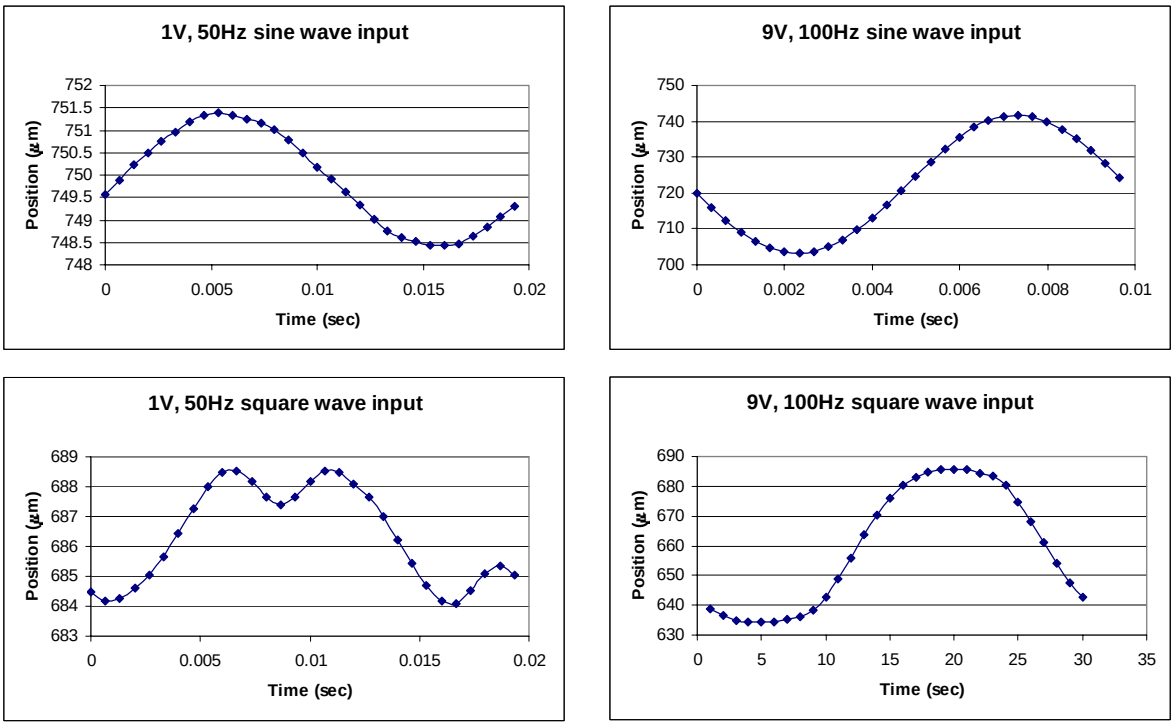

Figure 3.13. Averaged path of PZT tip as a function of input.

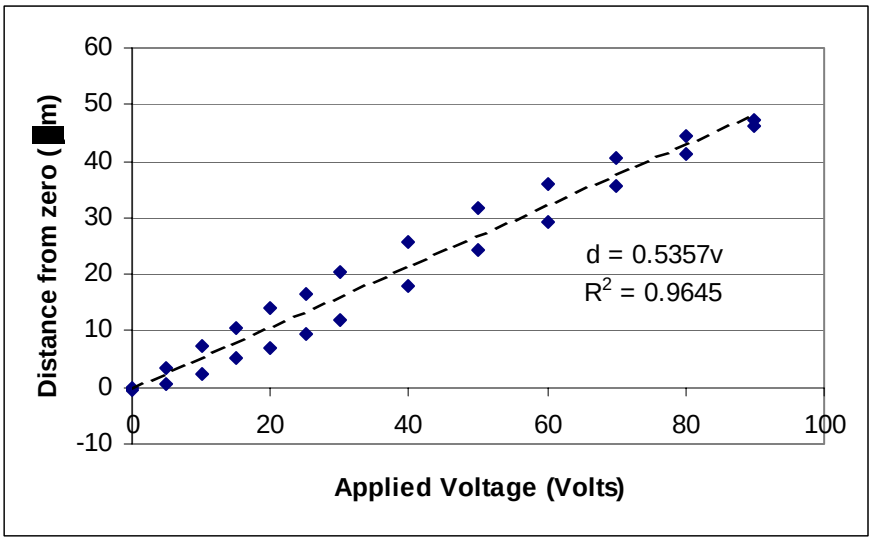

Figure 3.14. Position of PZT tip as a function of DC voltage input. There is notable hysterisis, with the position being below the average when voltage is increasing, and above the average when voltage is decreasing. The average position is equal to 0.5357 times the applied voltage.

In addition to sine and square wave tests, static displacement tests were conducted to test positioning accuracy of the PZT. A DC voltage was sent directly from the amplifier to the PZT, and the position relative to 0 volts was noted. This was done from 0 to 90 volts—the operational range of the PZT. Figure 3.14 summarizes the results. It can be seen that there is a bit of hysterisis. Averaging the data, and taking a least squares fit, the position of the PZT relative to any voltage can be predicted.

It should be noted that the sine and square waves of 1V, 3V, and 9V (which correspond to 10V, 30V, and 90V after being amplified) result in smaller amplitude movement than the DC voltage. Figure 3.15 illustrates this. A closer examination of the PZT's movement resulting from the AC signals reveals the reason.

The capacitance probe data was monitored for several seconds while the PZT was moving, resulting in thousands of cycles of data. A few hundred cycles were averaged to show the PZT's position at a specific time during each AC cycle. It can be seen in Fig. 3.13 that the motion due to a sine wave input is rather sinusoidal. However, motion due to a square wave is anything but square. This is because after a sudden change in input voltage, the PZT overshot its target, then

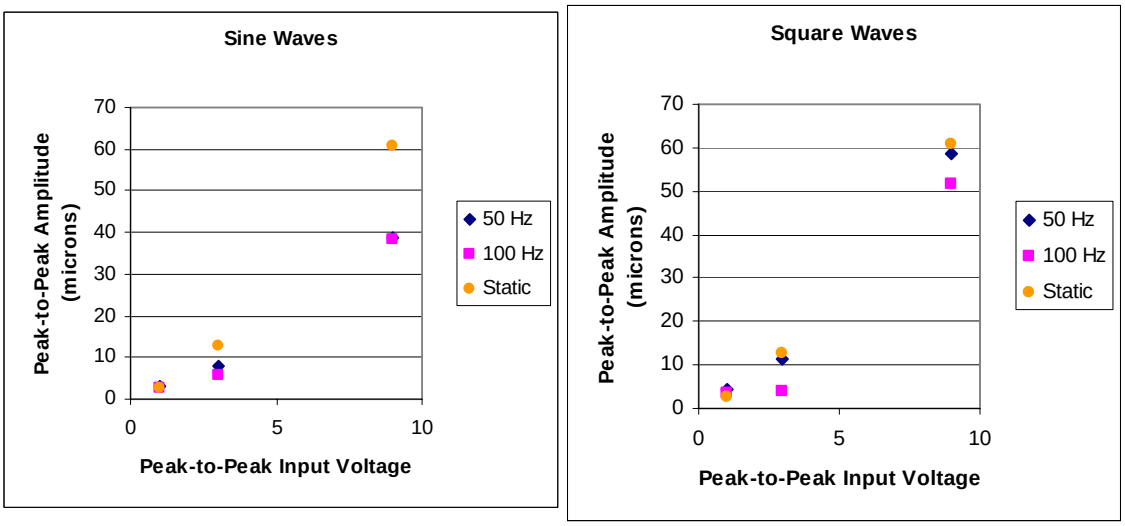

Figure 3.15. PZT amplitude is plotted against the applied voltage amplitude for sine and square inputs. The amplitudes are all smaller for the AC signals than for the DC voltage (or static) input, though the square input shows less deviation. Also, the PZT amplitude decreases with increasing input frequency.

corrected but overshot in the opposite direction, etc., resulting in an oscillation. But before the position reached steady state, the input signal dropped suddenly, and the oscillation repeated.

The limited range of the capacitance probe meant that while it was ideal to examine the short movement of the z-stage, the larger movements needed to be tested with a laser interferometer. The z-stage was moved in 50mm increments over its entire 250mm range at the maximum speed of 2mm/sec, and the stage position was recorded at the end of each move by the laser interferometer. The average error over these moves was 12µm or 0.025%. Movements of 1mm were checked at 0.1mm/sec and 0.01mm/sec, and resulted in positioning errors of less than 1µm. These long-scale errors were important to know, but they are not necessarily indicative of the micro-EDM process, which uses slower feeds over a limited range of motion. These shorter movements of the z-stage at speeds more characteristic of micro-EDM were checked with a capacitance probe. The largest positioning error was a 2% overshoot on a move of 10µm at 1µm/sec (the slowest speed investigated), and all errors on moves of 50µm or shorter were less than 1µm. A summary of the errors can be seen in Table 3.3.

Table 3.3: Actual distances moved by the z-stage for three distance commands (left) at three different velocities (top). Standard deviations are all 0.2μm.

	10μm/sec	**5μm/sec**	**1μm/sec**
100μm	104.9μm	104.4μm	---
10μm	9.9μm	9.8μm	9.6μm
1μm	---	0.3μm	0.3μm

The data in Table 3.3 indicate that issuing a move of only 1μm would not be executed properly and that decreasing the velocity did not improve the accuracy. In addition to the positioning experiments, the capacitance probe was used to collect data while the z-stage and PZT were motionless, i.e. noise. The standard deviation of this data was observed to be 0.2 μm. All of the positions discussed above had standard deviations of 0.2 μm or smaller, and did not indicate any overshoot greater than this 0.2μm noise. This means that the positioning of the z-stage and PZT could never be known to better than ±0.3μm (root mean square sum of 0.2μm in z-stage and 0.2μm in PZT).

3.3 The Peripherals

3.3.1 Tooling

Tool electrodes were chosen to mimic small hole making micro-EDM systems while maintaining simple geometries. The tool electrode material was a 140μm tungsten cylinder. Tungsten is a common and excellent tool electrode because of its high melting point and generally good thermal properties. The workpiece electrodes were discs of pure metals, covering a large range of melting points (Aluminum, Copper, Iron, Molybdenum, Titanium, Tungsten, and Zinc), or small sheets of 304 stainless steel. All were prepared by polishing to a mirror finish. These high smoothness values made inspecting the results of micro-EDM discharges more apparent. The workpiece electrode was clamped to a workpiece mount using a small toe clamp and bolt (see Fig. 3.16) to prevent and movement during the machining process. The power supply was connected to the tool electrode with a spade clip and bolt at the tool holder, and to the workpiece

electrode by similar method at the workpiece mount. Since both the tool holder and workpiece mount were metallic, they easily transferred the power supply charges to the tool and workpiece.

3.3.2 Dielectric Unit

The machining environment, where both electrodes resided, was inside a machining vessel that contained the dielectric liquid (see Fig. 3.16). The vessel was a clear rectangular box made of plastic (Lexan), 140 mm wide, 200 mm long, and 130 mm deep. The vessel was filled with the dielectric fluid until both electrodes were completely submerged. Ionoplus (a synthetic oil, manufactured by Hirschmann GMGH, Fluorn-Wilnzeln, Germany, www.hirschmannusa.com) commonly used in die-sinking EDM and in some micro-EDM systems was used as the dielectric. The oil was cycled through a filter to keep the liquid clean and to keep it flowing. Flushing the dielectric fluid through the work zone can aid in removing more of the molten metal.

3.3.3 Measurement

The discharges were measured on a digital oscilloscope using a current probe. A Tektronix P6021 current probe (manufactured by Tektronix, Inc., Oregon, USA, www.tektronix.com) fitted over any wire in the circuit (the circuit was not broken to measure current) to measure the current flowing during a discharge, and a standard Tektronix 10x voltage probe measured the voltage.

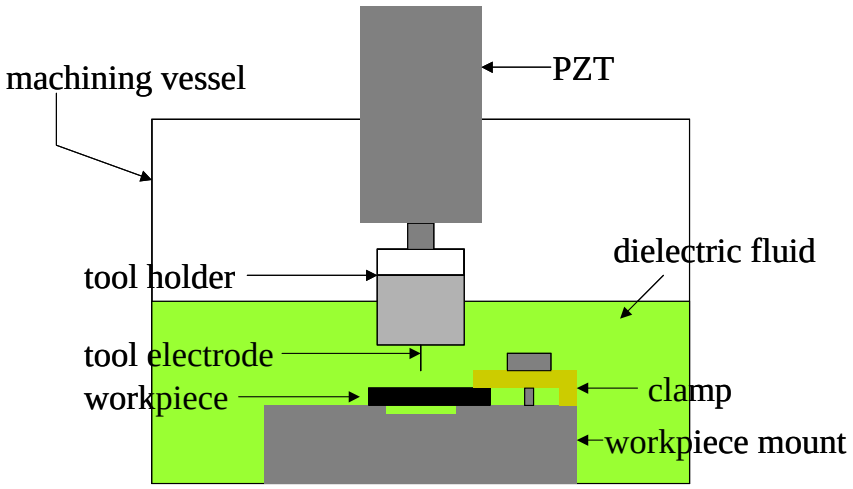

Figure 3.16. Schematic illustration of the machining area.

The probes were connected to a Tektronix DSA 602A digital signal analyzer (oscilloscope), which displayed the waveforms. The oscilloscope had a sampling rate of $2x10^9$ samples per second, which was necessary because current pulse widths were often as small as 50nsec. The DSA was equipped with a floppy disk for data storage, but waveforms were transferred to a PC using GPIB.

A Dell Pentium Pro 200 MHz computer was used to run National Instruments' LabVIEW (National Instruments Corporation, Texas, USA, www.ni.com) control software. Using the LabVIEW software, virtual instrument control panels were created to control the DC power supply, the oscilloscope, and motion system. The control program for the DSA also displayed the current waveforms, and saved the data in spreadsheet form, allowing for the waveforms to be recalled at a later time for analysis.

Because the machining vessel was clear, and the dielectric was at least translucent, a microscope could be used to view the machining area at 25x magnification, meaning the micro-EDM process could be monitored both electronically and visually.

4. Results

The goals set forth early in this project were to increase the general understanding of micro-EDM, increase the speed of micro-EDM, and establish exactly how small of a feature can be machined using micro-EDM. More insight into the micro-EDM process was obtained by examining the material removal resulting from individual discharges at energies typical of micro-EDM. In the preliminary stages of the project, the second and third goals were addressed by demonstrating that the experimental setup works well one dimension—drilling—and that the machining process was responsive to changes in the positioning conditions—the PZT. Positive results in these two regards mean that machining in three dimensions with directed, closed loop positioning control will allow all three goals to be achieved.

4.1 Single discharge experiments

The approach taken for this section is that breaking micro-EDM down to its most basic component, the unit or single discharge, is the best path for gaining knowledge and improving the understanding of the material removal process. This idea is based on the premise that material removal is the cumulative result of a sequence of discharges and therefore, studying the material removal characteristics of a single discharge and its relation to discharge parameters in a controlled way offers a path to a better understanding of micro-EDM. Investigating material removal by a single discharge allows machining parameters to be investigated in a more controlled manner. The main focal points of this study were applied voltage, pulse width (duration), and the combination of the two—applied energy.

The single discharges were made using the PFL by inserting a switch between the DC power supply and the coaxial cable (see Fig. 3.9). This switch could be closed to charge the line. After the switch was reopened, the line would hold the charge until the tool came close enough to the workpiece to create a spark and discharge the circuit. The tool was a 140μm Tungsten rod and the workpiece was a highly polished disc.

Plan views of the micro-EDM craters created by a single electrical discharge on a Copper workpiece (Fig. 4.1: table of three Cu craters with SEM, Zygo, and profiles) reveal that they are very similar to craters produced at larger energies (Greene 1974)—circular in shape surrounded by a rim of re-solidified metal. However, unlike the rough, jagged craters often seen at larger energies, the craters produced by micro-EDM appear rather smooth (see SEM images in Fig. 4.1). The profile, or cross-sectional, views are particularly revealing, showing that the rims of re-solidified metal are shorter in height than the depths of the craters, and that the craters are much more wide than they are deep. Thus the craters are not hemi-spheres, but spherical caps.

Settings	SEM Photo	Zygo Plan View	Zygo Profile View
200V, 250nsec	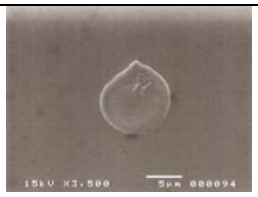	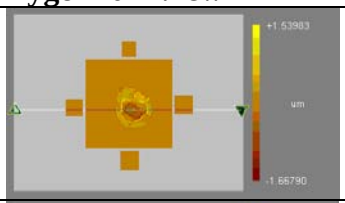	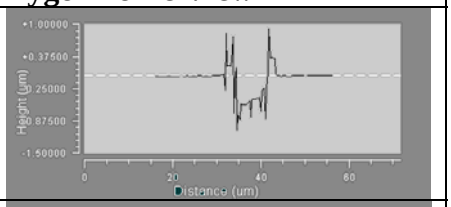
100V, 250nsec	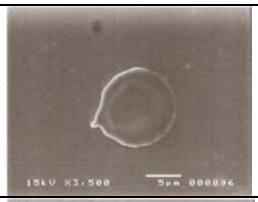	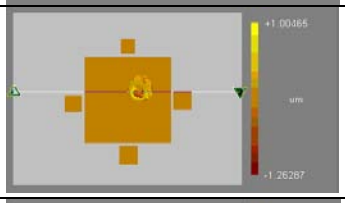	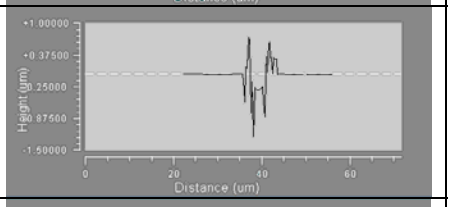
150V, 180nsec	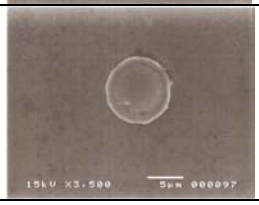	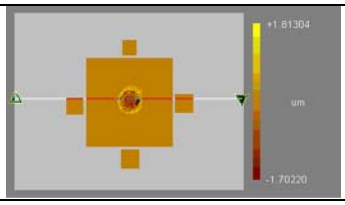	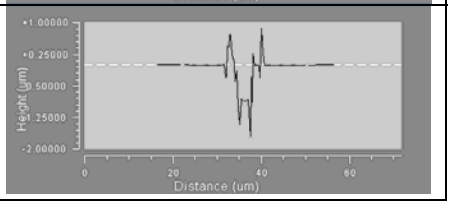

Figure 4.1. Individual craters created on Copper workpiece by various single discharges of micro-EDM.

The volumes of craters produced on the workpiece varied linearly with applied energy, increasing in size with increasing energy. A Zygo NewView 200 (manufactured by Zygo Corporation, Connecticut, USA, www.zygo.com) scanning white-light interferometer with MetroPro software was used to image the individual craters and determine the volume of material removed from the workpiece. As Fig. 4.2 illustrates, the volume data points fell along the same line regardless of whether the applied energy was varied by changing the pulse-width or the applied voltage. Figure 4.2 also shows a least squares fit applied to the copper volume data. The high quality of fit is indicated by the R^2 value of 0.98. Because of the circular shape of the craters, and the linear relationship volume has with applied energy, it might be intuitive

that crater diameter vary as the cube root of energy. This is indeed the case for the copper data, as seen in Fig. 4.3.

Pure metals in addition to Copper were chosen as workpieces because of their variety of melting points, and similar tests were conduced on them. These metals and their thermal properties can be found in Table 4.1. Least squares fits were applied to the volume data, and power law fits to the diameter data. Not all the fits were as tight as the Copper, but all were viewed as accurate. Crater size varied with material, meaning that craters created at the same energy on different metals were of different sizes.

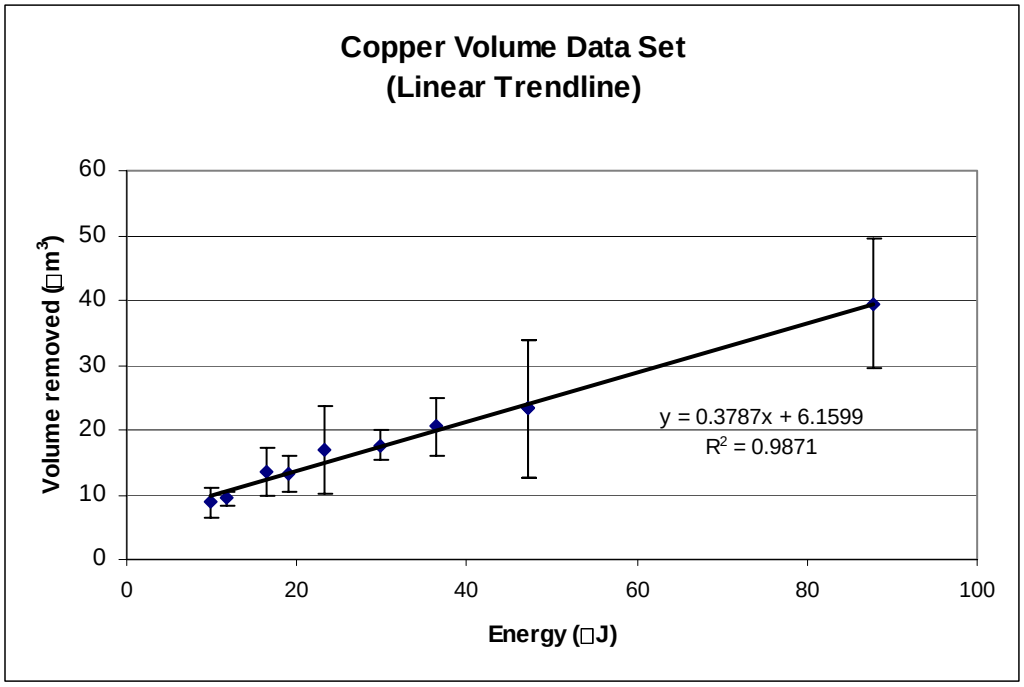

Figure 4.2. Volumetric removal of Copper due to single discharges of micro-EDM at various applied energies. Note that energy was varied by separately changing applied voltage and pulse width, but all data points still fall along the same line.

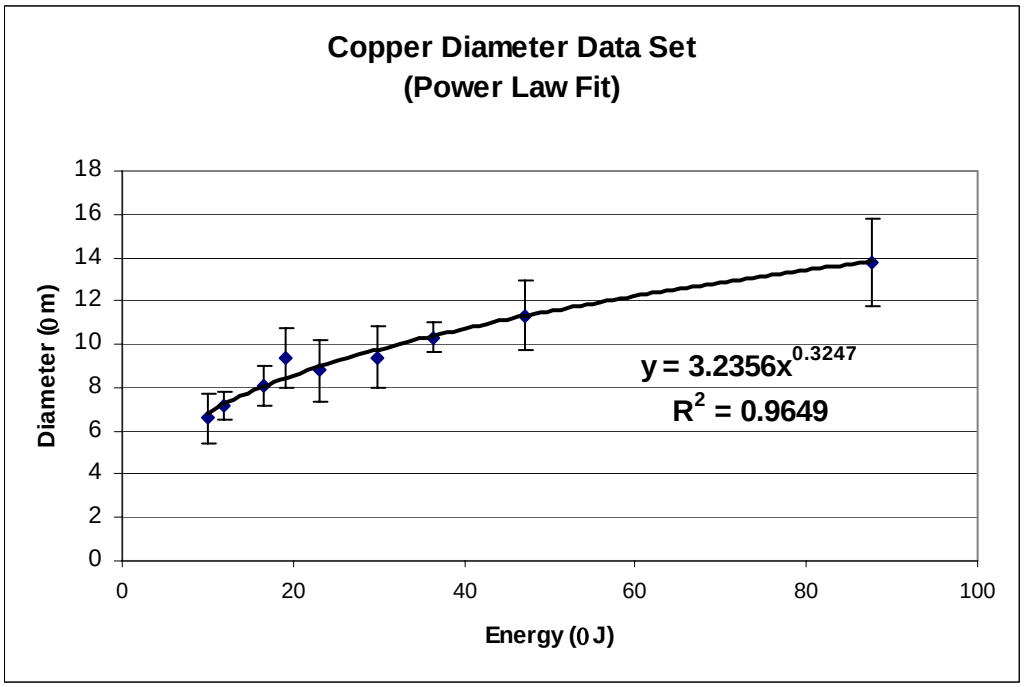

Figure 4.3. Diameters of craters created Copper due to single discharges of micro-EDM at various applied energies.

It was speculated that a material with higher melting point would have smaller craters than a material with lower melting point. However, predicting crater sizes, or even the relative sizes, has proven frustrating. Melting point is not the sole factor dictating the crater size variation, though most material removal rate equations vary only with the material's melting point (Jameson 2001, Weller 1984). It can be seen in Table 4.1 that craters created on Copper were smaller than craters created on Iron even though Copper has the lower melting point. Erosion Resistance Index, the product of melting point squared, thermal conductivity and specific heat, has been used (Reynaerts 1997) to determine how resistant a material is to spark erosion, making a material more suitable to be used as a tool electrode. The smaller the product, the larger the amount of material removed by a single discharge. This Index, however, is also flawed since the order of crater sizes was much different than the Index order. No other method of determining a material's relative EDM crater size could be found in the literature. Additionally, thermal models have not yet accurately predicted the size of craters created by micro-EDM discharges (Moylan 2000).

Table 4.1: Thermal properties of pure metal used in the single discharge experiments and volumetric removal at one specific applied energy.

Material	Melting Point, T_m (K)	Thermal Conductivity, k (W/m·K)	Specific Heat, c_v, (J/kg·K)	Erosion Resistance Index, C_m ($J^2/m \cdot kg \cdot sec \times 10^{11}$)	**Crater Volume at 47μJ (μm^3)**
Zinc	693	116	389	0.2	**174**
Aluminum	933	237	903	1.9	**87**
Copper	1358	401	385	2.8	**23**
Iron	1810	80	447	1.2	**37**
Titanium	1953	21	522	0.4	**20**
Molybdenum	2894	138	251	2.9	**19**
Tungsten	3660	174	132	3.1	**15**

4.2 Piezoelectric actuator experiments

The simplicity with which holes could be made using DC voltage through the PFL as a power supply meant it could be used to conduct experiments designed to demonstrate the importance of the PZT and motion control unit. Again, 200V applied voltage and 250nsec pulse-widths were used with the 140μm Tungsten tool to sink through 300μm of stainless steel. The voltage applied to the PZT and the frequency it was applied were varied. Specific values of each were chosen and holes were drilled at several different z-axis feed settings until the hole was completed in the smallest amount of time. If the z-axis is feeding too fast, the number of shorts, and therefore the number of "short retracts" increases. A larger number of "short retracts" means the tool actually has to travel farther, and therefore machining time might be larger for a faster feed with many shorts than a slower feed with few shorts. The values of PZT applied voltage and frequency along with the results of the tests are shown in Table 4.2. An optical micrograph of a hole cut using PZT settings of 3V and 100Hz is shown in Fig. 4.4.

Table 4.2: PZT parametric experiments and results.

PZT settings		Experiment results	
Applied Voltage	Frequency of oscillation of PZT	Time (min:sec)	Optimum Feed
3V	50Hz	22:10	0.25 μm/sec
3V	100Hz	18:38	0.30 μm/sec
3V	300Hz	12:26	0.45 μm/sec
1V	50Hz	~18:00*	0.30 μm/sec
6V	50Hz	~46:00*	0.15 μm/sec

* Tests stopped at 250μm because of different problems. Times are extrapolated to 300μm. The trends in the data can clearly be seen despite the tests' not finishing.

It is evident from Table 4.2 that machining time decreases when amplitude of PZT oscillation is decreased. Decreasing amplitude can be achieved by either decreasing applied voltage of the same frequency, or increasing frequency at the same amplitude (see Fig. 3.12). This is because discharges occur if the gap between the tool and the workpiece is small enough to break down the dielectric, i.e. the tool is in the machining zone. When the amplitude is too large, the tool moves in and out of the machining zone, meaning there are fewer discharges. When the amplitude is small, the tool stays in the machining zone, and discharging is much more consistent. When this occurs, the circuit was discharging at maximum frequency of approximately 3kHz, though discharge frequencies around 1 to 1.5kHz were more common.

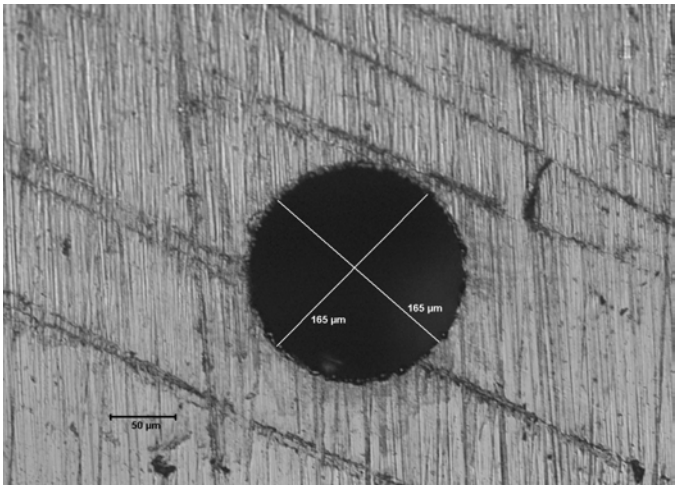

Figure 4.4. Optical micrograph of a hole made using the PFL as a power supply. The diagonal lines across the hole show the hole's diameter and that the hole is very round.

More rapid discharging cannot be achieved because RC circuits, like the PFL, are bound to recharge exponentially.

The contribution of vibration frequency is less evident, but noticeable. The hole cut with PZT applied voltage of 3V and frequency of 100Hz took approximately the same amount of time as the hole cut with PZT applied voltage of 1V and frequency of 50Hz. These results are of value because the former cut was accomplished in the same amount of time even though the PZT amplitude was significantly smaller for the latter cut. Decreasing the PZT vibration amplitude at a frequency of 100Hz to around 3μm should yield a machining time much less than 18 minutes. Another observation was made with regard to performance at lower frequency. A test was set up with a PZT applied voltage of 0.5V at a frequency of 50Hz, resulting in vibration amplitude of 1.5μm (as characterized by capacitance probe). This would be the same amplitude as the 3V, 300Hz test, only at a slower frequency. However, the test could not be completed because when the tool was fed forward, the tool electrode would weld to the workpiece after only a few discharges. While the vibration was sufficient to prevent this welding at 300Hz, it was not sufficient at 50Hz. The conclusion from these observations is that material removal over a period of time increases as PZT frequency increases.

4.3 Pulse power supply experiments

It was previously discussed in chapter 3 that, with all else being equal, the transistor based Purdue Pulse Power Supply (PPPS), with better control over discharge frequency, is a better option than an RC circuit and DC power supply that offers little control over how often the circuit discharges. However, since the PPPS had never been used before, its effectiveness needed to be demonstrated before any quantitative results could be measured.

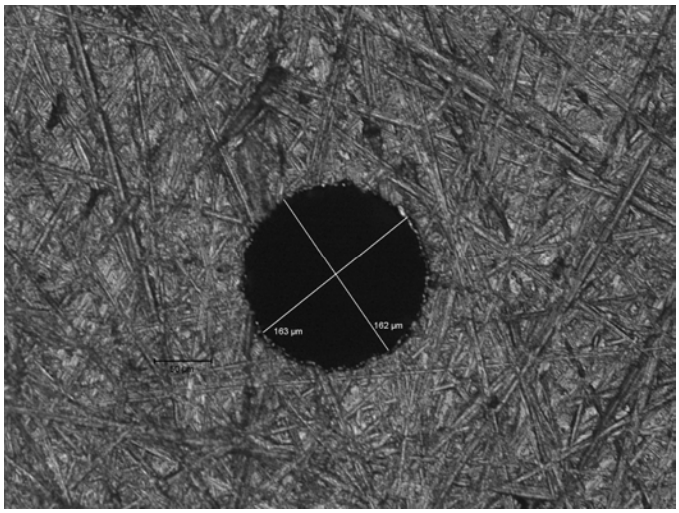

Figure 4.5. First hole made using the PPPS. This hole is very similar in size and shape to the hole made with the T-line.

The first hole made using the PPPS was done so with 100V applied voltage, 1A peak current setting, 1µsec pulse width, and a frequency of 10kHz. The hole shown in Fig. 4.5 shows that the hole made with the PPPS is very similar to the holes made with the T-line. This similarity is expected because the energy per discharge (discharge voltage times gap current times pulse duration, all of which were found during characterization of the PPPS) in this experiment, 85µJ, was very similar to the discharge energy used to make holes using the PFL, 88µJ. Examination of the diameter of the PPPS hole in Fig. 4.5 (165µm) shows exactly how similar this hole is to the PFL hole in Fig. 4.4 (165µm in diameter).

With the effectiveness of the PPPS demonstrated, a simple 2^k factorial design of experiments was drawn up to investigate the relative importance of the various settings of the PPPS. The parameters explored were applied voltage, pulse width, and frequency, meaning that k=3. Peak current was kept at a constant setting of 1A for all of the tests. Again, the same 140µm diameter Tungsten tool and 300µm thick steel workpiece were used. The PZT settings were a constant 100Hz vibration frequency and 3V peak-to-peak applied amplitude voltage. Holes were made using one particular set of parameters but at several z-axis feed rates until the fastest machining time was found. The parameter sets and experiment results are shown in Table 4.3, and optical micrographs of the holes are shown in Figure 4.6.

Table 4.3: Parametric study and results for Purdue Pulse Power Supply.

Power supply settings			Results		
	Pulse width	**Frequency**	**Time (min:sec)**	**Optimum Feed**	**Overburn**
100V	500nsec	10kHz	13:33	0.55µm/sec	9µm
100V	500nsec	20kHz	10:41	0.60µm/sec	10µm
100V	1µsec	10kHz	14:18	0.50µm/sec	11µm
100V	1µsec	20kHz	6:06	1.00µm/sec	13µm
200V	500nsec	10kHz	7:30	0.90µm/sec	9µm
200V	500nsec	20kHz	5:09	1.15µm/sec	10µm
200V	1µsec	10kHz	4:42	1.35µm/sec	10µm
200V	1µsec	20kHz	3:43	1.70µm/sec	12µm

An immediate observation from the above results is that with only a few exceptions, the holes machined with the PPPS system were completed much more quickly than those made by the PFL. The reason for this is that the PPPS creates many more discharges than the PFL does. As mentioned earlier, the discharge frequency of the PFL is not controlled, and the maximum frequency observed was ~3kHz, with more typical discharge frequencies of ~1.5kHz. The PPPS does not create a discharge every time it sends a pulse (there are a fair number of open circuits, especially at the beginning of the cut) but by sending pulses at a rate of 10 or 20kHz, the likelihood of having many more than 3000 discharges per second is very high.

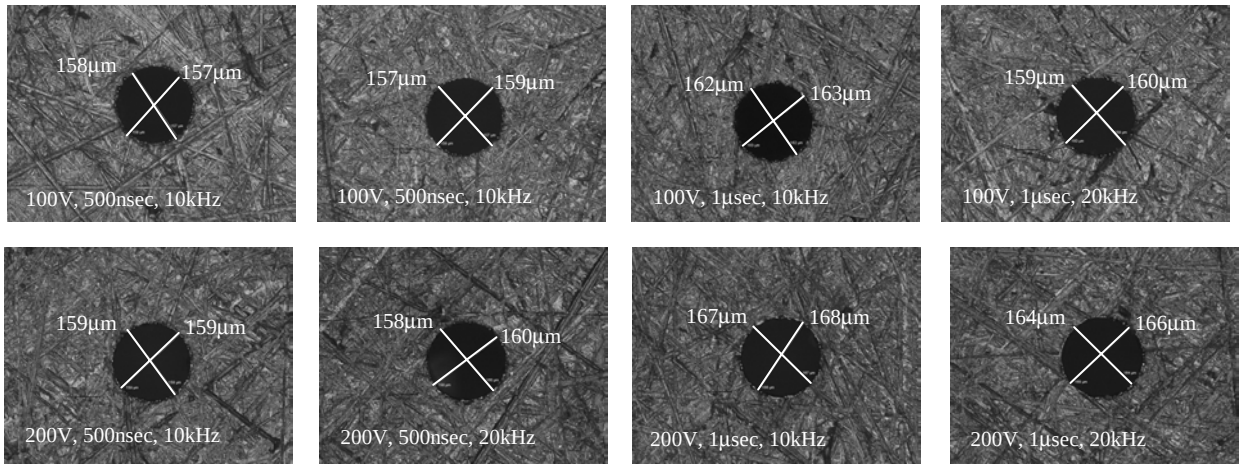

Figure 4.6. Results of PPPS parametric study. Diagonals show hole diameter. Tool was 140µm Tungsten post.

Since a 2^k factorial design of experiments was employed, statistical analysis of the results revealing the relative importance of each parameter, was rather simple. A typical analysis of variance method was carried out on the machining times (Montgomery 1994). The sum of squares for each of the main parameters and various combinations of the parameters were calculated. The sum of squares for the voltage was very high, 250,000sec^2, followed by frequency, 93,000sec^2, and pulse width, 29,000sec^2. None of the combination sums of squares exceeded 27,000sec^2. The fact that the voltage sum of squares was the largest by a significant amount means that changing the voltage has much more of an effect on machining time than changing pulse frequency or pulse width. Changing pulse frequency still has a noticeable effect on machining time, but the effect of changing pulse width is almost second order when compared to the other two, and is on par with the second order effects of parameter combinations.

Applied voltage dominating material removal rate when making holes does not agree with the single discharge data seen earlier. The plots of volumetric removal versus energy (Fig. 4.2) and crater diameter versus energy (Fig. 4.3) indicate that applied energy (the combination of voltage and pulse width) is the main driver of removal rate. Manipulating energy by changing the voltage only did not have a greater or lesser effect than changing pulse width only. The results in Table 4.3 indicate that this is not at all the case when using the PPPS to make holes.

4.4 Hole Morphology

These above conclusions concerning pulse width should not indicate that pulse width does not affect the machining process at all. On the contrary, when investigating the overburn on each hole, pulse width turns out to be the main parameter influencing this. Overburn, which is inherent to all EDM processes, is defined as the difference in size between the radius of the hole and the radius of the tool making the hole. When performing a similar statistical analysis on the overburn data, it is seen that pulse width has the greatest effect, followed by applied voltage (sum of squares for pulse width equals 8μm^2 and 5μm^2 for applied voltage). No other energy parameter or combination has any affect on the sizes of the holes.

While it is evident from Figs. 4.5 and 4.6 that the PPPS holes are very round, they do have some taper to them. For the majority of tests, the machining was stopped when the tool barely broke

through the bottom of the workpiece. However, in two of tests (the 100V-1µsec-10kHz and 200V-1µsec-10kHz tests), machining was extended to allow the tool to protrude well below the bottom of the workpiece. When the diameters at the bottoms of the holes (Fig. 4.7) are compared with those at the tops (Fig. 4.6), it is evident that since the diameters at the tops are larger than the diameters at the bottoms, there is a slight amount of taper to the holes. This taper results from the EDM debris being ejected out of the top of a hole along the outside of the tool. Sometimes discharges occur between the debris and the workpiece, slightly enlarging the hole at the top. Since the debris moves out from the bottom to the top of the hole, this phenomenon is observed more at the top of the hole, resulting in a slight taper.

4.5 Conclusions

The experimental setup, discussed in the previous section and pivotal to success of this project, has yielded high quality and encouraging results. The previously untested Purdue Pulse Power Supply did an excellent job of small-hole making. The operational parameters are comparable with the existing micro-EDM technology, and are variable enough to allow fruitful experiments to be conducted. Preliminary experiments have shown that machining time can be influenced by high-speed positioning of the tool electrode using the PZT, or by improvements in the motion control in general. Further improvements in this area will likely lead to further improvements in machining time and efficiency.

In a more quantitative regard, experiments have shown that machining time can be decreased in

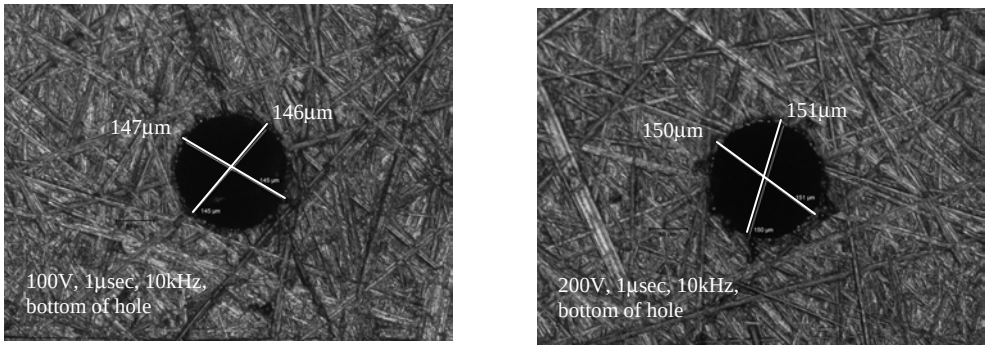

Figure 4.7. The smaller diameters at the bottoms of holes show that there is a slight taper.

several ways. Using a small PZT amplitude at higher frequencies significantly increases the amount of time the tool is in the machining zone, and therefore results in faster machining times. Additionally, increasing the applied voltage, pulse frequency, or pulse-width can reduce machining time, with voltage having the most dramatic effect.

5. FUTURE WORK

Since manipulating the PZT in open loop control reduced machining time, it is hypothesized that operating the PZT in closed loop can further reduce machining time. Specifically, the voltage between the power supply, whether it be the PPPS or the T-line, and ground can be compared with the voltage between the tool electrode and the workpiece. The control circuit described in U.S. patent 6,385,500 (Hebbar et al.) does this by averaging the two voltages over a small period of time, dividing the two voltages, and sending the output of that division back to the PZT amplifier to reposition the tool. If the voltage between the tool and workpiece is zero, the electrodes are shorted and the output of the control circuit is a voltage that will quickly retract the tool to allow machining to continue. If the two voltages are exactly the same, the tool is too far away from the workpiece to create a spark. In this case the control circuit will output such that the tool is moved closer to the workpiece, but at a speed such that overshoot will be minimized and the tool will not crash into the workpiece. Between these two extremes, comparison of the two voltages, and changes in the output, can be used to evaluate the micro-EDM process, and the tool can be repositioned to improve material removal rates. The control circuit described in the patent was designed to operate with a small-hole making EDM system that used different machining parameters than those typical of this study. Changes will be made to the circuit to accommodate the differences. Additionally, the control circuit used in this study should be robust enough to operate with both the PPPS and the T-line being used as the power supply. Holes made using the improved controller will be compared to the holes made with open circuit control for both speed and quality.

When the hole-making experiments are exhausted, two new linear stages will be added to allow machining in three dimensions. A simple control program will be written in LabVIEW to allow slots and simple three-dimensional shapes to be machined. Newport Corporation's (California, USA, www.newport.com) P850F linear actuators arranged in an x, y-axis configuration provide an excellent solution for this setup because these actuators are very accurate and are compatible with the z-stage. These actuators use backlash corrected ball screws and servomotors, have resolution of less than 1µm and accuracy of 5µm for 100mm of travel. LabVIEW programs

already controlling the z-stage are also equipped to operate the x-, and y-stages either independently or as a unit.

When simple three-dimensional shapes can be machined, guidelines on the minimum feature size attainable by the experimental setup may be established. The intricacies of machining in more than one dimensions will be dealt with while learning to use the new stages. These intricacies will determine the exact method of machining. But the method that will more than likely be employed will be very similar to the Uniform Wear Method as outlined in existing literature (Yu 1998).

After the success of machining in one dimensions—making holes—the next logical step is machining in two dimensions, or the making of slots. Various techniques of two-dimensional machining will be attempted to find the most effective. Once slots are easily produced, two slots will be machined parallel to each other and space between the slots will be determined and compared to the programmed value. The distance between parallel slots can be continually decreased until the two slots blend together as one. The smallest distance at which two distinct slots still exist provides an accurate estimate of the smallest feature machinable by the micro-EDM process using the given machine settings. Power supply parameters like voltage and pulse width, positioning variables like feed, and tool electrode diameters can be varied to demonstrate how each affects slot production and the minimum feature attainable. This data, combined with already existing data and knowledge, will enable estimation or a map of design rules at any given settings.

6. REFERENCES

1. D.M. Allen (2000), "Microelectrodischarge machining for MEMS applications," **IEE Seminar on Demonstrated Micromachining Technologies for Industry**, pp 6/1-6/4.

2. D. Allen, H. Almond, and P. Logan (2000), "A technical comparison of micro-electrodischarge machining, microdrilling, and copper vapour laser machining for the fabrication of ink jet nozzles," **Proceeding of the SPIE Symposium on Design, Test, Integration and Packaging of MEMS/MOEMS**, v4019, pp 531-540.

3. H. Almond, J. Bhogal, and D.M. Allen (1999), "A positional accuracy study of a micro-EDM machine," **Proceedings of the SPIE Symposium on Design, Test, and Microfabrication of MEMS and MOEMS**, v3680, pp 1113-1124.

4. W. Ehrfeld, H. Lehr, F. Michel, and A. Wolf (1996), "Micro electro discharge machining as a technology in micromachining," **Proceedings of the SPIE Micromachining and Microfabrication Symposium**, v2879, pp 332-337.

5. J.E. Greene and J.L. Guerrero-Alvarez (1974), "Electro-erosion of metal surfaces," **Metallurgical Transactions**, v5, pp 695-706.

6. R.R. Hebbar, R. Ramanujam, and S. Chandrasekar (2002), "Hybrid servomechanism for micro-electrical discharge machining," **United States Patent #6,385,500**.

7. P.-H. Heeren, D. Reynaerts, H. Van Brussel, C. Beuret, O. Larson, and A. Bertholds (1997), "Microstructuring of silicon by electro-discharge machining (EDM)—part II: applications," **Sensors and Actuators A**, v61, pp 379-386.

8. M.-G. Her and F.-T. Weng (2001), "micromachining by EDM process of stainless steel by tungsten carbide electrode," **Journal of the Chinese Society of Mechanical Engineers**, v22 no2, pp 171-175.

9. T. Huguchi, K. Furutani, Y. Yamagata, Ktakeda, and H. Makino (1991), "Development of pocket-sized electro-discharge machine," **Annals of the CIRP**, v40, pp 203-206.

10. E. C. Jameson (2001), **Electrical Discharge Machining**, Society of Manufacturing Engineers, Michigan.

11. K. Kagaya, Y. Oishi, and K. Yoda (1986), "Micro-electrodischarge machining using water as a working fluid—I: micro-hole drilling," **Precision Engineering**, v8 no3, pp 157-162.

12. H. Lowe, W. Ehrfled, and J. Diebel (1997), “Ultraprecision microelectroforming of metal and metal alloys,” **Proceedings of the SPIE, Micromachining and Microfabrication Symposium**, v3223, p 168-175.

13. T. Masaki, K. Kawata, and T. Masuzawa (1990), “Micro electro-discharge machining and its applications,” **Proceedings of the IEEE: MEMS**, pp 21-26.

14. T. Masuzawa, M. Fujino, and K. Kobayashi (1985), “Wire electro-discharge grinding for micro-machining,” **Annals of the CIRP**, v34 no1, pp 431-434.

15. T. Masuzawa, M. Fujino, K. Kobayashi, T. Sazuki, and H. Fujino (1986), “Wire electro-discharge grinding system for machining very fine rods,” **International Conference on Computer-Aided Production Engineering** (Edinburgh), pp 247-254.

16. T. Masuzawa, J. Tsukamoto, and M. Fujino (1989), “Drilling of Deep Microholes by EDM,” **Annals of the CIRP**, v38, pp 195-198.

17. T. Masuzawa, C.-L. Kuo, and M. Fujino (1994), “A combined electrical machining process for micro-nozzle fabrication,” **Annals of the CIRP**, v43, pp 189-192.

18. T. Masuzawa and H.K. Tönshoff (1997), “Three-dimensional micromachining by machine tools,” **Annals of the CIRP**, v46 no2, pp 621-628.

19. D.C. Montgomery and G.C. Runger, (1994), **Applied Statistics and Probability for Engineers**, John Wiley & Sons, Inc. New York

20. D. Reynaerts, P.-H. Heeren, and H. Van Brussel (1997), “Microstructuring of silicon by electro-discharge machining (EDM)—part I: theory,” **Sensors and Actuators A**, v60, p212-218.

21. D. Reynaerts, W. Meeusen, and H. Van Brussel (1998), “Machining of three-dimensional microstructures in solicon by electro-discharge machining,” **Sensors and Actuators A**, v67, pp 159-165.

22. N. Ravi and S.X. Chuan (2002), “The effects of electro-discharge machining block electrode method for microelectrode machining,” **Journal of Micromechanics and Microengineering**, v12, pp532-540.

23. N. Ravi and H. Huang (2002), “Fabrication of symmetrical section microfeatures using the electro-discharge machining block electrode method,” **Journal of Micromechanics and Microengineering**, v12, pp 905-910.

24. K.P. Rajurkar, V.V. Navelkar, and J.E. Springer (1987), “High-speed pulse train analysis for real-time EDM control,” **SME Technical Paper**.

25. K.P. Rujurkar and Z.Y. Yu (2000), “3D micro-EDM using CAD/CAM,” **Annals of the CIRP**, v49 no1, pp 127-130.

26. K.P. Rajurkar and Z.Y. Yu (2000), “Micro-EDM can produce micro parts,” **Manufacturing Engineering**, v11, pp 68-75.

27. T. Sato, T. Mizutani, K. Youemochi, and K. Kawata (1986), “The development of an electrodischarge machine for micro-hole boring,” **Precision Engineering**, v8 no3, pp 163-168.

28. N. Shibaike, H. Takeuchi, K. Nakamura, and N. Shimizu (2000), “Approach to higher reliability in 3D micro-mechanisms,” **Proceedings of the SPIE: Micromachining Technology for Micro-Optics**, v4179, pp 170-179.

29. R. Snoeys, D. Dauw, and M. Jennes (1982), “Survey of adaptive control and detection systems,” **Annals of the CIRP**, v31 no2, pp 483-489.

30. G. Spur and J. Schönbeck (1993), “Anode erosion in wire-EDM—a theoretical model,” **Annals of the CIRP**, v42 no1, pp 253-256.

31. K. Takahata, N. Shibaike, and H. Guekel (1999), “A novel micro electro discharge machining method using electrodes fabricated by the LIGA process,” **Proceedings of the IEEE: MEMS**, pp 238-243.

32. K. Takahata, N. Shibaike, and H. Guckel (2000), “High-aspect-ratio WC-Co microstructure produced by the combination of LIGA and micro-EDM,” **Microsystem Technologies**, v6, pp 175-178.

33. K. Takahata and Y.B. Gianchandani (2001), “Batch mode micro-EDM for high-density and high throughput micromachining,” **Proceedings of the IEEE: MEMS**, pp 72-75.

34. K. Takahata and Y.B. Gianchandani (2002), “Batch mode micro-electro-discharge machining,” **Journal of MEMS**, v11 no2, pp 102-110.

35. K. Takahata, S. Aoki, and T. Sato (1997), “Fine surface finishing method for 3-dimensional micro structures,” **IEICE Transactions on Electronics**, vE80-C no2, pp 291-296.

36. E. Uhlmann, G. Spur, N.A. Daus, and U. Doll (1999), “Application of micro-EDM in the machining of micro structured forming tools,” **SME Technical Paper MF 99-285**.

37. E. J. Weller (1984), **Nontraditional Machining Processes**, Society of Manufacturing Engineers, Michigan.

38. F.-T. Weng and M.-G. Her (2002), “Study of the batch production of micro parts using the EDM process,” **International Journal of Advanced Manufacturing Technology**, v19, pp 266-270.

39. A. Wolf, W. Ehrfeld, F. Michel, O. Koch, S. Preub, H. Soultan, and H.P. Graber (1998), “Application of new actuator and vision control systems for micro electro discharge machining,” **Proceedings of the SPIE: Conference on Intelligent Systems in Design and Manufacturing**, v3517, pp 149-158.

40. B.H. Yan, A.C. Wang, C.Y. Huang, and F.Y. Huang (2002), “Study of precision micro-holes in borosilicate glass using micro EDM combined with ultrasonic vibration machining,” **International Journal of Machine Tool and Manufacture**, v42, pp 1105-1112.

41. S.H. Yeo and G.G. Yap (2001), “A feasibility study on the micro-electro-discharge machining process for photomask fabrication,” **International Journal of Manufacturing Technology**, v18, pp 7-11.

42. L. Yong, G. Min, L. Fang, and Z. Zhaoying (2002), “Research of micro electro discharge machining equipment and process techniques,” **Chinese Journal of Mechanical Engineering**, v15 no2, pp 177-181.

43. Z.Y. Yu, T. Masuzawa, and M. Fujino (1998), “Micro-EDM for three-dimensional cavities—development of uniform wear method,” **Annals of the CIRP**, v47 no1, pp 169-172.

44. Z. Yu and K.P. Rujurkar (2000), “Generation of complex micro cavities by micro-EDM,” **Transactions of NAMRI/SME**, vXXVIII, pp 233-238.

Distribution:

3	MS 0311	Gilbert Benavides, 2616
1	MS 1245	Ed Boucheron, 2432
1	MS 0130	Joe Polito, 10700
1	MS 0123	LDRD, Donna Chavez, 1011
1	MS 9018	Central Technical Files, 8945-1
2	MS 0899	Technical Library, 9616